MPZL2, Encoding the Epithelial Junctional Protein Myelin Protein Zero-like 2, Is Essential for Hearing in Man and Mouse

Mieke Wesdorp,[1,2,3,15] Silvia Murillo-Cuesta,[4,5,6,15] Theo Peters,[1,3] Adelaida M. Celaya,[4,5] Anne Oonk,[1] Margit Schraders,[1,3] Jaap Oostrik,[1,3] Elena Gomez-Rosas,[5,7] Andy J. Beynon,[1] Bas P. Hartel,[1,3] Kees Okkersen,[3,8] Hans J.P.M. Koenen,[9] Jack Weeda,[10] Stefan Lelieveld,[2,11] Nicol C. Voermans,[3,8] Irma Joosten,[9] Carel B. Hoyng,[3,10] Peter Lichtner,[12] Henricus P.M. Kunst,[1,13] Ilse Feenstra,[11] Suzanne E. de Bruijn,[11] DOOFNL Consortium,[3,11] Ronald J.C. Admiraal,[1] Helger G. Yntema,[11] Erwin van Wijk,[1,3] Ignacio del Castillo,[5,7] Pau Serra,[14] Isabel Varela-Nieto,[4,5,6,16] Ronald J.E. Pennings,[1,3,16] and Hannie Kremer[1,3,11,16,*]

In a Dutch consanguineous family with recessively inherited nonsyndromic hearing impairment (HI), homozygosity mapping combined with whole-exome sequencing revealed a *MPZL2* homozygous truncating variant, c.72del (p.Ile24Metfs*22). By screening a cohort of phenotype-matched subjects and a cohort of HI subjects in whom WES had been performed previously, we identified two additional families with biallelic truncating variants of *MPZL2*. Affected individuals demonstrated symmetric, progressive, mild to moderate sensorineural HI. Onset of HI was in the first decade, and high-frequency hearing was more severely affected. There was no vestibular involvement. *MPZL2* encodes myelin protein zero-like 2, an adhesion molecule that mediates epithelial cell-cell interactions in several (developing) tissues. Involvement of MPZL2 in hearing was confirmed by audiometric evaluation of *Mpzl2*-mutant mice. These displayed early-onset progressive sensorineural HI that was more pronounced in the high frequencies. Histological analysis of adult mutant mice demonstrated an altered organization of outer hair cells and supporting cells and degeneration of the organ of Corti. In addition, we observed mild degeneration of spiral ganglion neurons, and this degeneration was most pronounced at the cochlear base. Although MPZL2 is known to function in cell adhesion in several tissues, no phenotypes other than HI were found to be associated with MPZL2 defects. This indicates that MPZL2 has a unique function in the inner ear. The present study suggests that deleterious variants of *Mplz2/MPZL2* affect adhesion of the inner-ear epithelium and result in loss of structural integrity of the organ of Corti and progressive degeneration of hair cells, supporting cells, and spiral ganglion neurons.

Introduction

The identification of genes associated with hereditary nonsyndromic hearing impairment (NSHI) has accelerated in the last decade with the introduction of next-generation sequencing. But despite the fact that currently more than 100 deafness-associated genes are known (Hereditary Hearing loss Homepage; see Web Resources), more than 60 percent of subjects with hereditary NSHI still cannot be genetically diagnosed.[1–6] These individuals and their relatives receive suboptimal care because of insufficient counseling on prognosis and recurrence risk. In addition, syndromic features can be overlooked, or in the opposite case, health-care providers perform unnecessary and costly tests to screen for additional symptoms that are not present.

Given the number of deafness loci for which the associated gene is not known yet (Hereditary Hearing loss Homepage), it is estimated that many monogenic forms of NSHI still await identification. Discovery of these NSHI-associated genes will contribute to the full understanding of the complex physiology of hearing. However, the search for genes associated with deafness has become more challenging because most frequently involved genes are already known and those that remain are most likely involved in less than 1 percent of the cases, or even in only one or a few families with NSHI. Also, identification of deleterious variant(s) in a single family in a gene not

[1]Hearing and Genes Division, Department of Otorhinolaryngology, Radboud University Medical Center, 6500 HB Nijmegen, the Netherlands; [2]The Radboud Institute for Molecular Life Sciences, Radboud University Medical Center, 6500 HB Nijmegen, the Netherlands; [3]Donders Institute for Brain, Cognition and Behavior, Radboud University Medical Center, 6500 HB Nijmegen, the Netherlands; [4]Institute of Biomedical Research "Alberto Sols," Spanish National Research Council-Autonomous University of Madrid, 28029 Madrid, Spain; [5]Center for Biomedical Network Research in Rare Diseases, Institute of Health Carlos III, 28029 Madrid, Spain; [6]Hospital La Paz Institute for Health Research, 28029 Madrid, Spain; [7]Servicio de Genetica, Hospital Universitario Ramon y Cajal, Instituto Ramón y Cajal de Investigación Sanitaria, Madrid, Spain; [8]Department of Neurology, Radboud University Medical Center, 6500 HB Nijmegen, the Netherlands; [9]Laboratory of Medical Immunology, Department of Laboratory Medicine, Radboud University Medical Center, 6500 HB Nijmegen, the Netherlands; [10]Department of Ophthalmology, Radboud University Medical Center, 6500 HB Nijmegen, the Netherlands; [11]Department of Human Genetics, Radboud University Medical Center, 6500 HB Nijmegen, the Netherlands; [12]Institute of Human Genetics, Helmholtz Zentrum München, Neuherberg, Germany; [13]Radboud Institute of Health Sciences, Radboud University Medical Center, 6500 HB Nijmegen, the Netherlands; [14]Institut d'Investigacions Biomèdiques August Pi i Sunyer (IDIBAPS), 08036 Barcelona, Spain
[15]These authors contributed equally to this work
[16]These authors contributed equally to this work
*Correspondence: hannie.kremer@radboudumc.nl
https://doi.org/10.1016/j.ajhg.2018.05.011.

yet associated with NSHI is insufficient proof for causality. Functional studies and animal models are important tools for providing evidence for involvement of the identified gene in hearing.[7,8]

In this study, we report the identification of an NSHI-associated gene, *MPZL2* (MIM: 604873), by combining homozygosity mapping and whole-exome sequencing (WES) of a family of Dutch origin. Subsequent screening of a phenotype-matched cohort and analysis of WES data of genetically undiagnosed individuals with NSHI led to the identification of two additional families of Turkish origin with truncating variants in *MPZL2*. We characterized the phenotype of affected individuals and of mice with an intragenic deletion of *Mpzl2*.[9] In addition, we observed histological abnormalities in the cochleae of the mutant mice.

Subjects and Methods

Subject Evaluation

This study was approved by the medical ethics committee of the Radboud University Medical Center and is in accordance with the principles of the World Medical Association Declaration of Helsinki. Written informed consent was obtained from all participants or their legal representatives.

Medical history was obtained from all participants via a questionnaire focusing on hearing and balance, as well as possible acquired causes of HI. Otoscopy was performed in all subjects so that the tympanic membrane and aeration of the middle ear could be assessed. Pure-tone audiometry was performed in a sound-treated room according to current standards. Air conduction thresholds were determined at 0.25, 0.5, 1, 2, 4, and 8 kHz in dB HL. Bone conduction thresholds were determined at 0.5, 1, 2, 4, and 8 kHz in dB HL, so that conductive HI could be excluded. HI was described according to the recommendations of the GENDEAF study group.[10] Progression of HI was evaluated by cross-sectional linear regression analysis of last-visit audiograms of the better-hearing ear and used for construction of age-related typical audiograms (ARTAs), as described previously.[11] Individual progression of HI was calculated for each frequency with longitudinal linear regression analyses via GraphPad Prism 6.0. Tympanometry was performed, and click-evoked ABR and otoacoustic emissions (OAEs) were obtained according to current standards. Contralateral and ipsilateral acoustic reflexes were measured at 0.5, 1, 2, and 4 kHz up to the loudness discomfort level. Speech-perception thresholds and maximum speech-recognition scores were determined with speech audiometry, which was performed in a sound-treated room with standard monosyllabic consonant-vowel-consonant Dutch word lists.[12]

Vestibular function was assessed with electronystagmography (ENG) rotary chair stimulation and caloric irrigation testing according to current standards. Additionally, cervical vestibular evoked myogenic potentials (cVEMPs) and video head impulse tests (vHITs) were performed so that sacculus and vestibulo-ocular reflex (VOR) functionality, respectively, could be assessed. For assessing the presence of polyneuropathy, standardized neurological screening was performed in accordance with a predefined protocol (Supplemental Methods). Screening for Immunological and corneal defects was performed as described in the Supplemental Methods.

Description of Subject Cohorts

Two cohorts, a phenotype-based cohort and a WES cohort, were screened for the presence of *MPZL2* variants. The phenotype-based cohort consisted of 120 individuals with a phenotype comparable to that of individuals of family W05-682, affected members of which demonstrated sensorineural NSHI and a flat, cookie-bite or downsloping audiogram configuration. Of these, 57 subjects were Dutch and displayed stable, mild to severe NSHI; 63 subjects were Spanish and displayed mild to profound NSHI. Only isolated cases and subjects with suspected autosomal-recessive inheritance were included. All subjects were previously tested for a phenotype-based selection of single genes.

The WES cohort consisted of 270 subjects who had presumed recessive HI and for whom WES had been performed previously in a clinical diagnostic setting. In these subjects, pathogenic variants in genes known to be associated with HI (gene panels DGD 200614, DG2.4x or DG2.5/2.6) were excluded by targeted analysis of WES data, as described previously.[6] Gene lists and coverage in WES are available at the Genome Diagnostics Radboudumc homepage (see Web Resources). Variants in genes of the panels were classified according to the guidelines from the Association for Clinical Genetic Science and the Dutch Society of Clinical Genetic Laboratory Specialists.[13] Subjects were not preselected on the basis of their HI phenotype.

Homozygosity Mapping

Genomic DNA was isolated from peripheral blood lymphocytes by standard procedures. The samples of subjects II:1 and II:3 of family W05-682 (Figure 1) were genotyped with the Affymetrix mapping 250K SNP array according to the manufacturer's protocol (Santa Clara, CA, USA). Genotype calling was performed with the Genotyping Console software (Affymetrix) under default settings. Homozygosity mapping was performed with the online tool HomozygosityMapper[14] so that significant shared homozygous regions could be identified. Other shared homozygous regions larger than 1 Mb and regions of shared heterozygous genotypes were identified manually.

VNTR Marker Analysis

Genotyping of variable number of tandem repeat (VNTR) markers was performed by DNA amplification with touchdown PCR and analysis on an ABI Prism 3730 Genetic Analyzer (Applied Biosystems). Primers for amplification of VNTR loci were designed with Primer3Plus. Genetic location of the markers was derived online from the Marshfield genetic map, and marker order was confirmed in the human genome assembly GRCh37/hg19. Alleles were assigned with GeneMapper v.4.0 software according to the manufacturer's protocol (Applied Biosystems).

Whole Exome Sequencing

Exome DNA was enriched using the Agilent SureSelect version 4, 5, or 6 kit. WES was performed on an Illumina HiSeq system by BGI-Europe (Denmark). The index cases of families W05-682, W16-0195, and W16-0451 were reanalyzed for an updated gene panel for HI (panel DG2.11) as described in the section "Description of Subject Cohorts." Copy-number variation (CNV) was evaluated by depth-of-coverage analysis with CONIFER as described.[15,16] Mean $\geq$20x coverage per sample was 95.9% to 96.5% of the enriched regions. Variants were regarded as rare if the minor-allele frequency (MAF) was $\leq$1% in the in-house database of ~15,000 exomes and if the MAF was $\leq$1% in gnomAD.

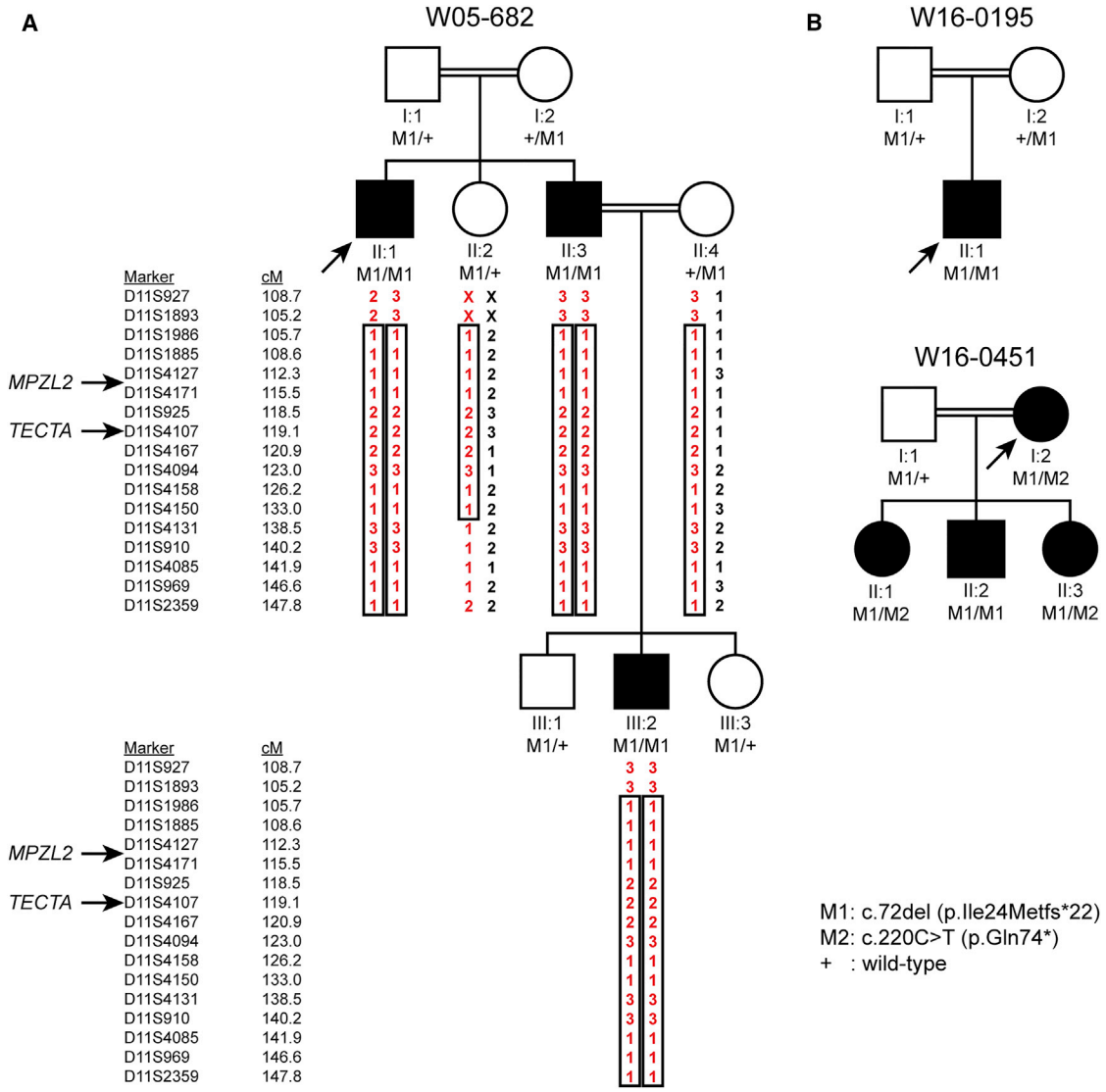

Figure 1. Pedigrees, VNTR Genotypes and Segregation of Variants of *MPZL2*
(A) Genotypes of VNTR markers and segregation of identified truncating variants of *MPZL2* in family W05-682. Besides *MPZL2*, *TECTA* (DFNB21) is also located within the homozygous region shared by the affected individuals. Pathogenic variants in the coding and intronic regions of *TECTA* were excluded.
(B) Pedigrees and segregation analyses of two additional families with deleterious variants in *MPZL2*. Index cases are indicated by arrows. Double lines indicate consanguinity (for extended pedigrees, see Figure S1).

Prediction of deleterious effects of missense variants and prediction of an effect on splicing were performed as described in the Supplemental Methods.

Sanger Sequencing

Primers for amplification of exons and exon-flanking intronic sequences of *MPZL2* (GenBank: NM_005797.3) and *TECTA* (ENST00000392793, MIM: 602574) and primers for mRNA analysis of *TECTA* were designed with Primer3Plus and Oligo Primer Analysis Software. Amplification by PCR was performed under standard conditions. DNA isolated from peripheral blood samples was employed for analysis of exons and exon-flanking intronic DNA of *MPZL2* and *TECTA*. For *TECTA* mRNA analysis, total RNA was isolated from Epstein-Barr-virus-transformed lymphoblastoid cells of affected subjects II:1 and II:3 of family W05-682 with the NucleoSpin RNA II kit (Machery Nagel) according to the manufacturer's protocol. Poly A^+ RNA was isolated from total RNA with the OligoTEX mRNA Spin Column kit (QIAGEN) according to the manufacturer's protocol. Subsequently, cDNA synthesis was performed with the iScript cDNA Synthesis Kit (Bio-Rad Laboratories) and 0.5 μg poly A^+ RNA as a starting material, according to the manufacturer's protocol. PCRs were performed on 2 μL cDNA with Taq DNA polymerase (Roche). PCR fragments were purified with ExoI/FastAP or ExoSAP-IT (Thermo Fisher Scientific) in accordance with manufacturers' protocols. Sequence analysis was performed with the ABI PRISM BigDye Terminator Cycle Sequencing v.2.0 Ready Reaction kit and analyzed with the ABI PRISM 3730 DNA analyzer or the 3130 Genetic Analyzer (Applied Biosystems). Possibly deleterious effects of the identified variants on the MPZL2 and TECTA proteins and on splicing were predicted with Alamut Visual

(Interactive Biosoftware). Primer sequences and PCR conditions are provided in Table S1.

Quantitative PCR Analysis for Identification of Intragenic Deletions and Determination of *MPZL2* Expression in Human Tissues

Genomic quantitative PCR (qPCR) was performed as described in the Supplemental Methods. For analysis of transcript levels, total RNA derived from fetal heart, skeletal muscle, lung, brain, colon, kidney, stomach, spleen, and thymus and from adult skeletal muscle, liver, duodenum, stomach, spleen, thymus, and testis was purchased from Stratagene. Adult heart, lung, brain, kidney, bone marrow, and placenta total RNA was purchased from BioChain. In addition, total RNA was isolated from fetal cochlea (8 weeks of gestation) as described previously.[17] Subsequently, cDNA synthesis was performed with the SuperScript cDNA Synthesis Kit (Thermo Fisher Scientific) and 2 μg total RNA as starting material, according to the manufacturer's protocol. Specification on primer design, the qPCR system, and reaction mixtures are indicated above and in the Supplemental Methods. Primer sequences and conditions are provided in Table S1. The human beta glucuronidase gene (*GUSB,* MIM: 611499) was employed as a reference gene. All reactions were performed in duplicate. Relative gene expression levels were determined with the delta-delta Ct method.[18]

Audiometric Characterization of *Mpzl2*-Mutant Mice

Hearing was evaluated in C57BL6J wild-type (WT) and *Mpzl2*-mutant mice.[9] In these mutant mice, exons 2 and 3 of *Mpzl2* were deleted by standard gene-targeting methods.[9] This is predicted to result in an in-frame deletion of the coding sequences for amino acid residues 20–145, encompassing part of the signal sequence and the majority of the extracellular region of the 215 residue MPZL2 protein (*cf.* Figure S1). The strain was described as $Mpzl2^{ko/ko}$, although RT-PCR on liver RNA and Sanger sequencing of the amplicon confirmed transcript splicing of exon 1 to exon 4 as the only detectable splicing event in the mutant mice (P.S., unpublished data). The presence of the shortened protein in tissues of the mutant mice remains to be determined.

Auditory brainstem responses (ABRs) were registered in 4-, 8-, and 12-week-old mice (n = 5 per genotype and age group), essentially as reported by Cediel et al. (2006)[19] with the modifications reported by Murillo-Cuesta et al. (2015).[20] In brief, ABR recordings were obtained under anesthesia with ketamine (75 mg/kg, Imalgene, Merial) and xylacine (5 mg/kg, Rompun, Bayer). Click (0.1 ms, 30 pps rate) and tone-burst stimuli (8, 16, 20, 28, and 40 kHz, 5 ms, 50 pps rate) were generated with SigGenRP software (Tucker-Davis Technologies). Stimuli were presented from 90 to 10 dB, relative to sound pressure level (dB SPL) in 5–10 dB SPL steps with a MF1 speaker (TDT). The electrical responses were amplified, recorded, and averaged, and hearing thresholds were determined in the ABR recordings. Amplitudes of ABR waves I, II, and IV and interpeak latencies of peaks I-II, II-IV, and I-IV were analyzed for 70 dB SPL click stimuli.

Statistical analysis was performed with IBM SPSS 23.0 software. Nonparametric Mann-Whitney U tests were used for compaing ABR parameters between genotypes because of the small sample sizes. Differences were considered significant if $p < 0.05$.

Animal experiments were conducted in accordance with Spanish and European legislation and approved by the local bioethics committees.

Histology and Immunohistochemistry of Cochleae from Wild-Type and *Mpzl2*-Mutant Mice

Histology and immunohistochemistry were performed according to standard protocols, which are detailed in the Supplemental Methods. Antibodies used were the following: primary antibodies, rabbit anti-Kir4.1 (AB5818 Chemicon), rat anti-ZO-1 (sc-33725, Santa Cruz); rabbit anti-KCNQ1 (sc-20816, Santa Cruz), rabbit anti-Myosin VIIa (25-6790, Proteus), and goat anti-SOX2 (sc-17320, Santa Cruz). Rabbit anti-MPZL2, raised against the complete protein (11787-1-AP, Proteintech), goat anti-Collagen IV (1340-01, SouthernBiotech), and mouse anti-Na^+-K^+ATPase α1 (α6F, Developmental Studies Hybridoma Bank). The following served as secondary antibodies: Alexa Fluor (AF) conjugated immunoglobulins (Molecular Probes): AF 568-goat anti-rabbit (A11011), AF 488-donkey anti-goat (A11055), AF 488-goat anti-mouse (A11029), and AF 488-goat anti-rat (A11006).

Results

Homozygosity Mapping and WES Revealed Loss-of-Function Variants of *MPZL2*

Homozygosity mapping in a Dutch consanguineous family in which some members had autosomal-recessive NSHI (W05-682; Figure 1 and Figure S2) revealed a single significant homozygous region of 23.8 Mb on chromosome 11q23.1-q25, flanked by single-nucleotide polymorphisms (SNPs) rs4936310 and rs10458997 (Figure S3). VNTR marker analysis confirmed homozygosity of the region, and segregation of marker alleles in the family was compatible with linkage of the HI with a region that was flanked by D11S1893 at the centromeric side and included D11S2359 at the telomeric side (Figure 1A). D11S2359 is the most telomeric VNTR marker of chromosome 11q (UCSC Genome Browser, GRCh37/hg19). Combining VNTR marker and SNP data delimits the critical region to Chr11: 110,803,280–134,746,130. Two hundred and nine RefSeq genes, including *TECTA,* a known deafness-associated gene, have been annotated in this region (UCSC Genome Browser, GRCh37/hg19). However, pathogenic variants in *TECTA* were excluded by Sanger sequencing of all exons and exon-intron boundaries and by mRNA analysis. The homozygous region did not contain or overlap with any other genes or loci known to be associated with deafness. Fourteen additional homozygous regions larger than 1 Mb and shared by individuals II:1 and II:3 were identified (Table S2). There were no regions with shared heterozygous genotypes larger than 1 Mb.

As a next step, WES was performed in the index case (II:1) of family W05-682. The mean ≥20x coverage of genes in the homozygous region of chromosome 11q23.1–q25 was 98.1%. Variants were filtered as indicated in Figure S4 and classified as described in the Supplemental Methods (Table S3). Three rare homozygous variants in coding sequences and splice sites were present in the 23.8 Mb homozygous region. The *BSX* (MIM: 611074) variant c.263−5T>C (p.?) (GenBank: NM_001098168.1)

was predicted not to affect splicing. The missense *GRAMD1B* variant c.1111G>A (p.Val371Ile) (GenBank: NM_001286563.1) was predicted to be pathogenic by two of the four tools (Table S3). The third variant was a homozygous one-base-pair *MPZL2* deletion, c.72del (GenBank: NM_005797.3, Figure S5), that is predicted to result in premature termination of protein synthesis (p.Ile24Metfs*22). Because *MPZL2* was known to be transcribed in the cochlea at a significant level and the variant was truncating, it seemed the most promising candidate gene.[21,22] The *MPZL2* variant c.72del, with a global minor allele frequency (MAF) of 0.00077 and a MAF of 0.00127 in the non-Finnish European population, has only been reported heterozygously in gnomAD. The variant is reported to be most common in Ashkenazi Jews (MAF 0.00375). Segregation analysis by Sanger sequencing demonstrated co-segregation of the variant and HI in the family (Figure 1A), which was also true for the variants of *BSX* and *GRAMD1B*. Targeted analysis of WES data for a panel of 142 HI-associated genes revealed no other (likely) pathogenic variants. Also, no CNVs of the 142 HI-associated genes were detected, and thus no CNVs of *TECTA* were detected either. There were also no CNVs detected in the 23.8 Mb region. Exonic and flanking intronic sequences of *TECTA* were fully covered (≥15x). All detected variants of this gene are displayed in Table S4. None of the homozygous variants that occurred outside of the 23.8 Mb homozygous region and that were predicted to be pathogenic by two or more prediction tools co-segregated with the disease in the family (Table S3).

Identification of Additional Families with Deleterious *MPZL2* Variants

We addressed further involvement of *MPZL2* variants in recessive NSHI. A phenotype-based cohort of 120 unrelated probands with a phenotype similar to that of affected individuals in family W05-682 was screened for variants of *MPZL2*. This revealed the variant c.72del (p.Ile24Metfs*22) in a homozygous state in a family of Turkish origin, W16-0195. The variant was present heterozygously in the unaffected consanguineous parents (Figure 1B, Figure S5).

In two other individuals of the phenotype-based cohort, rare heterozygous *MPZL2* variants, namely c.268C>T (p.Arg90Trp) and c.544C>T (p.Arg182*), were identified. So that possible intragenic deletions of the second allele could be identified, genomic qPCR was performed for exons in which no heterozygous SNPs were detected (Table S5). No deletions were identified. Therefore, defects of *MPZL2* are unlikely to be causative of HI in these subjects. However, a deleterious variant in non-coding regions of the gene cannot be excluded.

Subsequently, data of a WES cohort of 270 genetically undiagnosed NSHI subjects were analyzed for rare *MPZL2* variants. This unveiled a third family, W16-0451, that was of Turkish origin and had truncating variants in *MPZL2*. Segregation analysis demonstrated that the c.72del and c.220C>T (p.Gln74*) variants were present in compound heterozygous state in the index case and that her affected offspring also carried biallelic truncating *MPZL2* variants (Figure 1B, Figure S5). The c.220C>T variant has been reported only heterozygously in gnomAD; it has a global MAF of 0.00038 and an MAF of 0.00003 in the non-Finnish European population, which represents a significant part of the Turkish ancestry.[23] The MAF of c.220C>T is 0.00515 in the East Asian population and 0.00016 in the South Asian population, as indicated in gnomAD. There is admixture of the Turkish population from Asia, mainly from West and Central Asia.[23] The c.220C>T variant has not been observed in other populations represented in gnomAD. WES data of the index case of family W16-0451 were reanalyzed for the updated panel of 142 HI-associated genes. This analysis was also performed for WES data of individual II:3. Neither of the two subjects had any potentially causative variants or CNVs of these genes and did not share rare CNVs in the remaining part of the exome. So that other variants that might underlie HI in family W16-0451 could be identified, rare variants homozygous in both individual I:2 and individual II:3 were evaluated, as were potentially compound heterozygous variants (Table S6). Segregation analysis of the candidate variants predicted to be pathogenic revealed that only the homozygous *PRDM2* (MIM: 601196) variant c.861_863del (GenBank: NM_012231.4; p.Asp287del) co-segregated with the disease. There were no variants that were homozygous in individual I:2 or II:3 and also potentially compound heterozygous in the other individual. Although the *PRDM2* transcript level in adult human cochlea (FPKM 58-73) is significant and is comparable to that of *MPZL2* (FPKM 35-83),[22] no HI has been reported for homozygous *Prdm2*-knockout mice (targeted) in the Mouse Genome Informatics (MGI) database, and ABR measurements of mice with an intragenic deletion of *Prdm2* revealed normal hearing, as reported by the International Mouse Phenotyping Consortium (IMPC). Therefore, the variant of *PRDM2* is unlikely to explain the HI in family W16-0451.

The c.72del *MPZL2* Variants Are Derived from a Common Founder

VNTR marker analysis was performed in families W05-682, W16-0195, and W16-0451 so that the haplotypes in the *MPZL2* region could be determined (Figure S6). All c.72del *MPZL2* alleles shared a haplotype of at least 0.5 Mb, delimited by markers D11S1341 and D11S4104, suggesting that it is a founder variant rather than a recurrent variant due to a mutational hotspot. Because the families have a different ethnic background, the c.72del variant is likely to be of ancient origin.

Clinical Characterization of Individuals with Pathogenic Variants of *MPZL2*

All affected and unaffected subjects of families W05-682, W16-0195, and W16-0451 underwent clinical examinations.

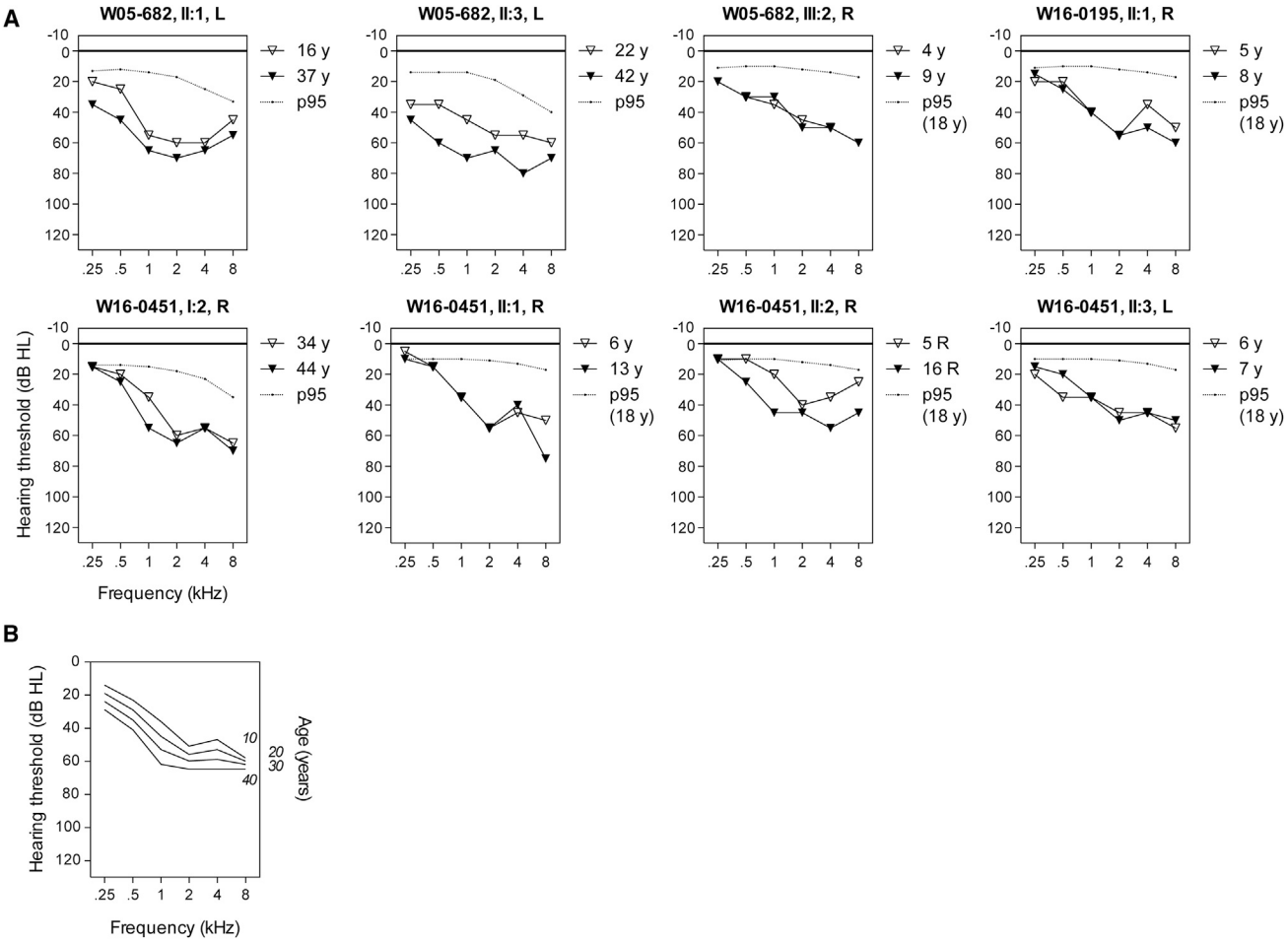

Figure 2. Audiometric Characterization of Families Affected by Pathogenic *MPZL2* Variants
(A) Air-conduction thresholds of the better-hearing ear of all affected individuals. The better-hearing ear was determined from calculations of the mean of the pure-tone thresholds for 0.5, 1, 2, and 4 kHz of the last audiogram. First-visit and last-visit audiograms are depicted. Subject II:1 of family W16-0451 was not able to participate in the clinical evaluation; only retrospective data for this subject were used for analysis. R, right ear; L, left ear.
(B) ARTA (age-related typical audiogram) constructed by cross-sectional linear-regression analysis of last-visit audiograms of all affected individuals (n = 8).

One of the siblings (II:1) of family W16-0451 was not able to participate in the current clinical evaluation; only retrospective data of this subject were used for analysis. History revealed that this individual previously underwent surgery for cholesteatoma of the left ear. Therefore, audiometric data of the right ear only were used for this study, and these data showed pure sensorineural HI. However, she also had osteogenesis imperfecta, which might contribute to her sensorineural HI. Nevertheless, her hearing thresholds were very similar to age-matched hearing thresholds of other affected family members, and therefore we decided to include her in the audiometric evaluations.

None of the affected subjects (family W05-682, II:1, II:3, and III:2; family W16-0195, II:1; family W16-0451, I:2, II:1, II:2, and II:3) demonstrated abnormalities on otoscopy and tympanometry (Table S7). Pure-tone audiometry of these individuals revealed no signs of conductive HI but did demonstrate a symmetric mild to moderate HI with a gently downsloping audiogram configuration for all of them (Figure 2A). The mean reported onset age of HI was 4 years (min–max: 3–9 years) (Table S8). Four affected individuals had a disturbed speech-language development, whereas development was normal in three cases and unknown in one case. Speech perception thresholds were lower than the pure-tone average thresholds at 0.5, 1, and 2 kHz, and maximum speech-recognition scores were 90%–100% for the better-hearing ear, both suggesting absence of retrocochlear pathology. Acoustic reflexes were present (both ipsilateral and contralateral) without decay, which also suggested an absence of retrocochlear pathology. OAEs could only be detected in individuals II:2 and II:3 of family W16-0451, for frequencies with hearing thresholds lower than 30 dB HL. This is indicative of residual function of cochlear OHCs.[24] OAEs were absent in all other affected subjects. The index cases of families W05-682 and W16-0195 displayed normal ABR wave latencies, which indicated normal auditory neural processing. Additional information on otologic and

audiometric evaluation of individual cases is provided in Table S7.

Individual longitudinal regression analyses of hearing thresholds revealed that HI was progressive in all affected adults. No progression could be demonstrated in the affected children, for whom follow-up time (1–11 years) was probably too short for significant progression to be established. Cross-sectional linear-regression analysis revealed progression of HI for all frequencies. The increase of hearing thresholds was significant at 1 kHz (0.8 dB/year), 2 kHz (0.5 dB/year), and 4 kHz (0.6 dB/year). In Figure 2B, the ARTA is depicted, which demonstrates gradual progression of HI.

None of the affected subjects or their parents reported vestibular symptoms, such as vertigo, dizziness, instability, or delayed motor development, except for the index case of family W16-0451 (I:2), who reported two periods of vertigo in the past without persisting complaints. Vestibular function was assessed in three of the hearing-impaired individuals (family W05-682, II:1; family W16-0451, I:2 and II:2), and normal to slightly hyperreactive vestibular responses were measured (Table S8).

Because *MPZL2* is highly homologous to *MPZ* (MIM: 159440), which is associated with distinct types of hereditary motor and sensory neuropathy,[25–31] we performed neurological screening of the affected individuals (family W05-682, II:1, II:3, and III:2; family W16-0195, II:1; and family W16-0451, I:2, II:2, and II:3). No symptoms or signs of neuropathy were present.

Hearing-impaired subjects were also screened for immunological abnormalities because *MPZL2* is involved in early thymocyte development.[32–34] None of them had symptoms of immunodeficiency, allergies, or autoimmune disease. CD4 and CD8 T cell counts, including double-positive ($CD4^+CD8^+$) and double-negative ($CD4^-CD8^-$) cell counts, as well as the CD4/CD8 ratios, were normal (Figure S7), indicating normal CD4 and CD8 expression on T cells.

Because gene expression studies have shown that *MPZL2* transcript levels are relatively high in the cornea of the eye (Ocular Tissue Database),[35] affected individuals were screened for corneal abnormalities. There were no eye problems, slit lamp biomicroscopy did not show abnormalities, and visual acuity was normal.

MPZL2 Is Expressed in Human Fetal Cochlea

The relative expression of *MPZL2* was determined in human fetal cochlea and various other fetal and adult human tissues (Figure S8). Because the fetal tissues were not derived from embryos of the same gestational age, mRNA transcript levels are not directly comparable. Among the tested fetal tissues, *MPZL2* expression was highest in the inner ear, where transcript levels were 70-fold higher than in skeletal muscle, which displayed the lowest detectable expression. Also, in all other fetal tissues *MPZL2* transcript levels were significantly lower than those in the inner ear. In the analysis of *MPZL2* expression in adult tissues, mRNA levels of *MPZL2* in the fetal inner ear were included for comparison. *MPZL2* mRNA was detected in all analyzed adult tissues, and the highest levels were in the thymus and lung, whose levels were in the range of those in fetal inner ear.

Mpzl2-Mutant Mice Are Hearing Impaired

Mpzl2-mutant mice showed early-onset progressive HI and significantly increased ABR thresholds in response to click and tone-burst stimuli in the ages studied, when these mice were compared to age-matched C57BL6J, normal-hearing wild-type mice. Four-week-old mutant mice showed a mild HI that affected the detection of click stimuli and pure-tone frequencies above 16 kHz (Figures 3A and 3B) at statistically significant higher thresholds ($p < 0.05$) than for wild-type mice. HI in mutant mice rapidly progressed to moderate and severe at the ages of 8 and 12 weeks, respectively, and these mice had statistically significant elevated thresholds for all tested stimuli in comparison to wild-type mice. At 12 weeks of age, ABR thresholds in response to 16–40 kHz are above 70 dB SPL in the mutant mice, whereas wild-type mice maintained normal hearing at thresholds below 30 dB SPL. Accordingly, significant alterations in ABR peak amplitudes, latencies, and interpeak latencies were observed in mutant mice. The maximum amplitudes of wave I, which represents cochlear activity, were approximately 30% lower in the knock-out animals than in the wild-type mice at all ages studied (Figure 3C), and differences reached significance in 4-week-old mice (Figure 3D). In addition, wave I peaks showed increased latencies in the mutants as compared to wild-type mice, which progressed over time. Peaks were increased in young animals (4 weeks old) at the level of intensity near the threshold, whereas in 12-week-old mice they were increased for all intensities tested (Figure 3E). Also, mutant mice showed significantly shorter interpeak latencies (IPLs) I-II, II-IV, and I-IV than wild-type mice (Figure 3F). These data suggest a compensatory central response to the delayed peripheral transmission, as already shown in the *Igf1* knockout.[36]

Mpzl2-Mutant Mice Display Alterations in Cell Organization and Cell Loss in the Organ of Corti

We evaluated the general cochlear cytoarchitecture in the basal, medial, and apical turns of the cochlea of 12-week-old mice (Figure 4 and Figure S9) to assess the integrity of the principal structures. Namely, we looked at the organ of Corti with inner and outer hair cells (IHCs and OHCs, respectively) responsible, respectively, for the mechanotransduction and amplification and tuning of the sound, and we looked at different types of supporting cells. Furthermore, we evaluated the spiral ganglion neurons that connect the hair cells with the central auditory pathway; the stria vascularis, involved in the formation of the high-potassium-containing endolymph, in the lateral wall; and the spiral ligament. Loss of hair and supporting cells of the organ of Corti (asterisk in

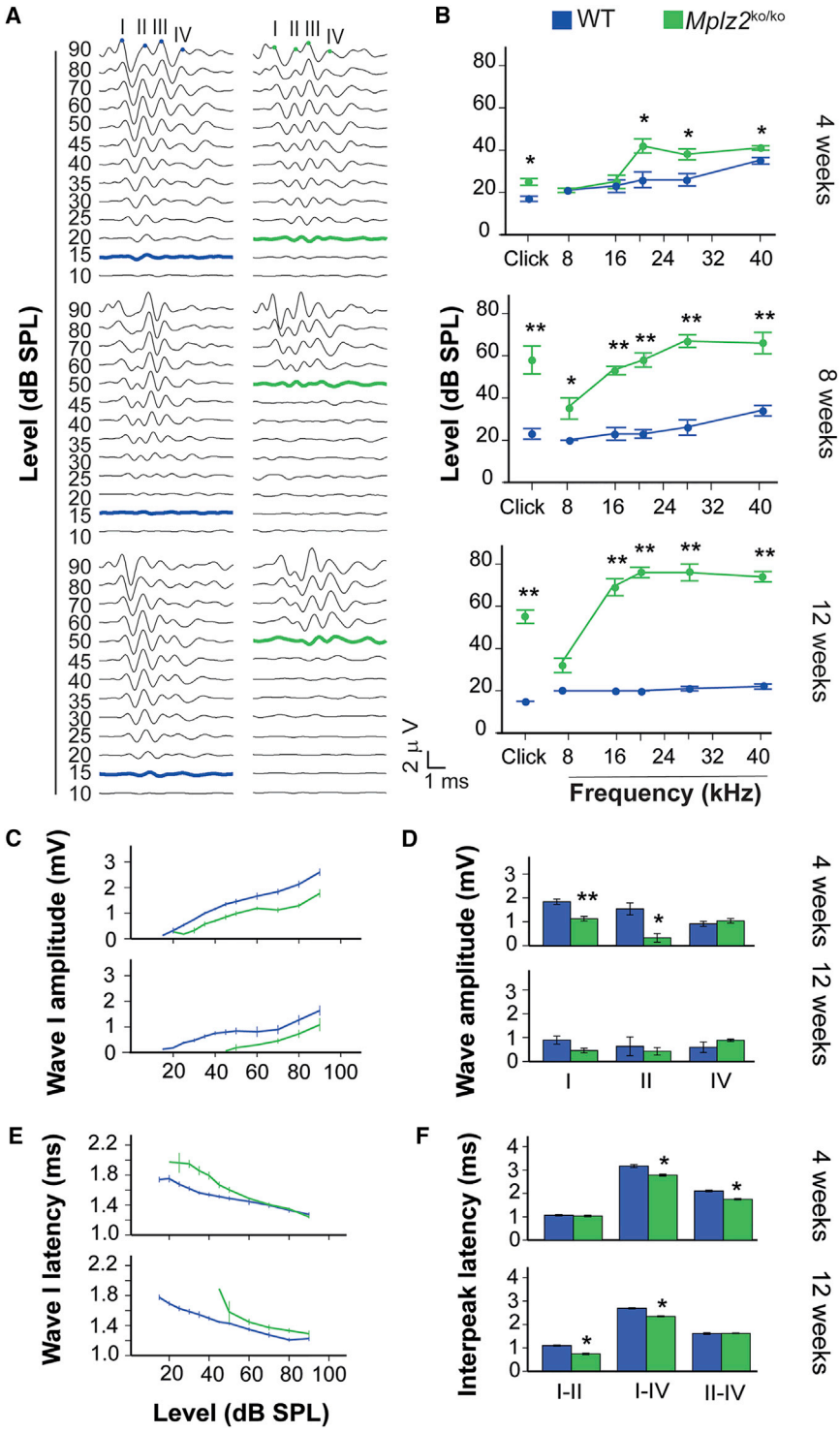

Figure 3. Hearing Phenotype of *Mpzl2*-Mutant (*Mpzl2*$^{ko/ko}$) Mice

(A) Representative click-evoked ABR recordings at decreasing intensities (dB SPL) in 4-, 8-, and 12-week-old wild-type and *Mpzl2*-mutant mice. Waves are labeled I–IV and reflect the evoked activity of the auditory nerve (I) and ascending points of the auditory pathway in the midbrain (II–IV). As the stimulus level is reduced, amplitudes of ABR waves decrease and latencies of waves increase. The lowest intensity at which the ABR-wave profile is higher than the background-noise signal is the threshold (bold line; WT, blue; *Mpzl2*-mutant mice, green).

(B) ABR thresholds, in response to click and 8–40 kHz tone bursts, of the different genotypes and age groups.

(C and E) ABR wave I amplitude/intensity (**C**) and latency/intensity (**E**) curves in response to click stimuli of increasing intensities were determined in 4- and 12-week-old wild-type and *Mpzl2*-mutant mice.

(D and F) Peak amplitude of ABR waves I, II, and IV (**D**) and interpeak latencies I-II, II-IV, and I-IV (**F**) in response to a 70 dB SPL click stimulus in 4- and 12-week-old wild-type and *Mpzl2*-mutant mice. Data are shown as means ± SEM. Statistical significance: *p < 0.05; **p < 0.01.

Figure S9D) and of neurons in the spiral ganglion (asterisks in Figure S9D-1) were observed in the basal cochlear turn of mutants, but not in wild-type mice. No evident structural abnormalities were seen in the stria vascularis or spiral ligament. Markers of the stria vascularis were not altered in mutant mice, as compared to age-matched wild-type animals (Figure S10).

A closer evaluation of the organ of Corti (Figure 4) showed clear differences between wild-type and *Mpzl2*-mutant mice at 12 weeks of age. At the basal turn of the cochlea, two mutant mice showed a flat epithelium at the basilar membrane; there was complete loss of hair and supporting cells (asterisks in Figure 4N and Figure 4O). At the medial and apical turns of the cochlea, hair and supporting cells were present in both genotypes, as were tunnel-forming inner and outer pillar cells (IPs and OPs, respectively) (Figure 4E). However, mutant mice showed an aberrant mosaic pattern of OHCs and supporting Deiters' cells (DCs; the spaces between OHCs had collapsed, and DC nuclei were displaced with respect to OHC nuclei (asterisks in Figures 4G, 4H, 4J–4L, and 4P).

Specific immunolabeling for Myosin VIIa and SOX2 evidenced that IHCs, OHCs, and supporting cells were present. Also, this analysis confirmed that mutant mice display a disorganized arrangement of OHCs and DCs in the apical (asterisks in Figures 5B and 5C) and middle (asterisk in Figure 5H) turns and that they display decreased numbers or an absence of all cell types in the basal turn of the cochlea (asterisks in Figures 5J–5L), in comparison to wild-type mice. Statistically significant

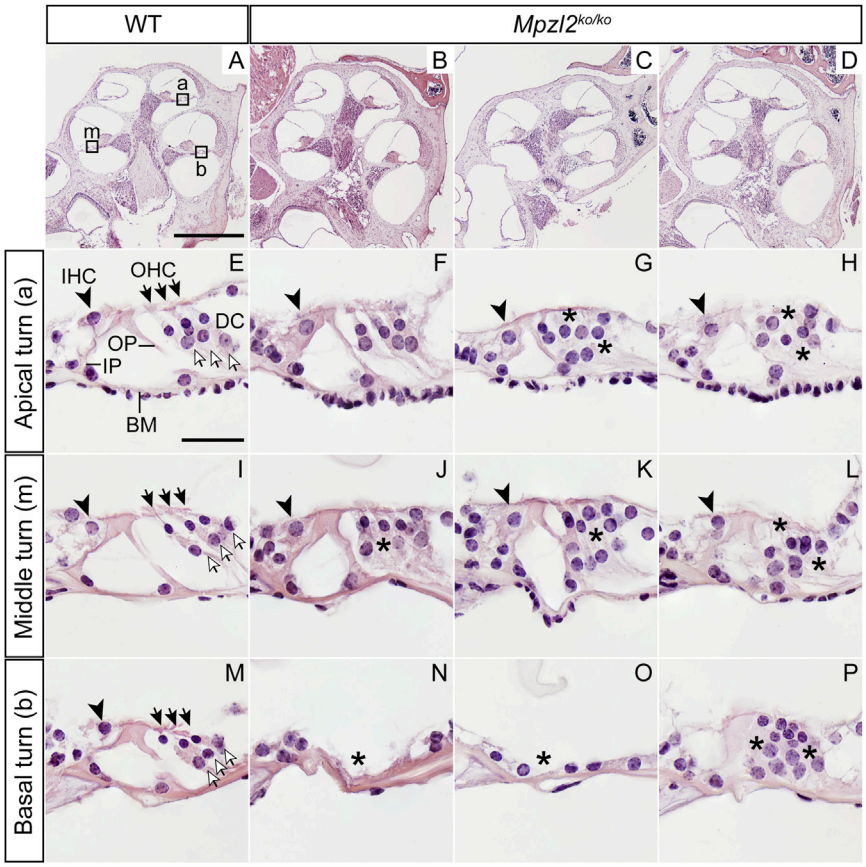

Figure 4. Cochlear Morphology of 12-Week-Old Wild-Type and *Mpzl2*-Mutant (*Mpzl2*$^{ko/ko}$) Mice

Microphotographs show representative midmodiolar cross sections of the cochlea from one representative wild-type mouse (A) and three *Mpzl2*-mutant mice (B–D). The apical (a), middle (m), and basal (b) organs of Corti are boxed in image (A). Close-ups of the organ of Corti from one wild-type mouse (E, I, and M) and three *Mpzl2*-mutant mice (F–H, J–L, and N–P) are shown. Arrowheads point to inner hair cells (IHCs), blackhead arrows to outer hair cells (OHCs), and arrows to Deiters cells (DCs). BM, basilar membrane; IP, inner pillar cell; and OP, outer pillar cell. Asterisks mark abnormalities. The scale bars represent 500 μm (A–D) and 25 μm (E–P).

differences were found in the number of OHCs in the basal turn only because of the differences in severity of the phenotype in mutant mice (Figure S11). At P4, no indications were obtained for an abnormal cellular organization in the developing organ of Corti (Figure S12).

Mouse MPZL2 Is Present in the Organ of Corti and the Stria Vascularis

Cochlear expression and localization of MPZL2 was assessed in wild-type mice at P4 by immunofluorescence, which revealed a signal in DCs and, most intensely, in the basal region of DCs in all three cochlear turns (Figure 6A and Figure S13). Staining of serial sections with anti-collagen IV suggests that MPZL2 is present where DCs contact the basilar membrane (Figures 6A and 6B). Weaker MPZL2 immunostaining is observed in both IHCs and OHCs (Figure 6A and Figure S13). In the stria vascularis, MPZL2 was detected in the basal cell layer, as confirmed by co-staining with anti-Na^{+}-K^{+}ATPase, which demarcates the intermediate cell layer (Figures 6C and 6D). Specificity of the anti-MPZL2 antibody was confirmed by analysis of cochleae of *Mpzl2*-mutant mice in the same experiments (Figure S13).

Discussion

This study provides evidence for the association of biallelic defects of *MPZL2* with recessively inherited sensorineural NSHI in humans and mice. Affected human subjects displayed moderate to severe, slowly progressive HI from the first decade onward, and intrafamilial and interfamilial phenotypic similarity was high. The functional and morphological inner-ear defects in *Mpzl2*-mutant mice provide important evidence for the causal relationship between *MPZL2* defects and HI in the studied families. This is further strengthened by the fact that HI of *Mpzl2*-mutant mice and affected family members was similar with regard to the early onset, the progressive nature, and the fact that high-frequency hearing was more severely affected than middle- or low-frequency hearing. The latter is reflected by the decreasing severity of disorganization and loss of OHCs and DCs from the cochlear base to apex.[37] For other genes that harbored variants that co-segregated with HI in families W05-682 and W16-0451 and were predicted to affect protein function, there are no supporting data for an association with HI. For *GRAMD1B* (W05-682), which is transcribed in adult human cochlea (FPKM 2.09-8.44[22]), no phenotyping information on mouse mutants is available in IMPC or MGI databases. No interactions of GRAMD1B with proteins encoded by genes associated with NSHI are reported (STRING or BioGRID).

TECTA (DFNB21, MIM: 603629) was located in the homozygous candidate region of family W05-682. Recessively inherited defects of *TECTA* can cause moderate-to-severe HI, although with a more flat audiogram configuration than observed in the presented families.[38,39] We scrutinized *TECTA* for defects in family W05-682, and we excluded (potentially) causative variants in the exonic sequences and splice sites of the gene. We did not obtain any indication for aberrant splicing that might result from deep intronic variants. Only variants in upstream or downstream sequences with a regulatory role

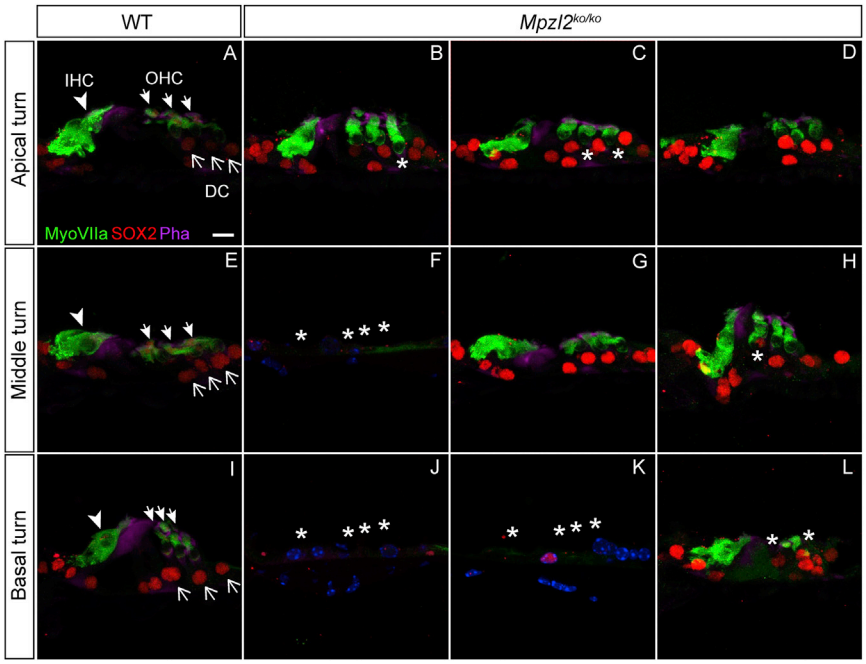

Figure 5. Organ-of-Corti Cytoarchitecture of Wild-Type and *Mpzl2*-Mutant (*Mpzl2*$^{ko/ko}$) Mice

Close-ups of the organ of Corti from representative frozen sections (10 μm) prepared from one representative wild-type mouse (A, E, and I) and three *Mpzl2*-mutant mice (B–D, F–H, and J–L). Hair cells and supporting cells were immunolabeled for Myosin VIIa (green) and SOX2 (red), respectively, in the apical, middle, and basal turns of the cochlea. Actin in the organ of Corti was stained with phalloidin (purple). Arrowheads point to inner hair cells (IHCs), whitehead arrows to outer hair cells (OHCs), and arrows to Deiters cells (DCs). Asterisks mark abnormalities. The scale bar represents 10 μm.

in transcription or intronic variants that could cause aberrant splicing specifically in the inner ear could have been missed.

The identified *MPLZ2* variants are the most common truncating variants in the gene; they have the highest gnomAD allele frequencies, of 0.0051 for c.220C>T in the East Asian population and 0.00375 for c.72del in the Ashkenazi Jews. For comparison, the c.2299delG founder mutation of *USH2A* (MIM: 608400) is most common in the latino population (0.0016) and has an allele frequency of 0.001 in non-Finnish Europeans. The most common cause of severe autosomal-recessive NSHI, the c.35delG mutation of *GJB2* (MIM: 121011), has a frequency of 0.0097 in non-Finnish Europeans in GnomAD. In light of this, the identification of defects of *MPZL2* as a cause of HI only now is surprising because the identified defects are expected to be important causes of HI in East Asia and in the Ashkenazi Jewish communities. Because research efforts were concentrated on severe-to-profound early-onset HI for many years, the association of *MPZL2* with HI might have remained undetected because of the mild-to-moderate severity of the HI. Also, because of the relatively mild HI, families might have a lower tendency to consult a genetic counselor or to participate in genetic studies than families in which more severe HI occurs. Furthermore, although not supported by our findings in the presented families, variants of *MPZL2* might have a reduced penetrance that could result from (common) modifying genetic variants.

The pLI score[40] of *MPZL2* is 0.00, which suggests that the gene is tolerant to loss-of-function variation. This is true for many of the HI-associated genes, e.g., *MYO7A* (MIM: 276903) and *USH2A*, which have the same pLI score of 0.00. The tool DOMINO[41] predicts that *MPZL2* is associated with a recessive rather than a dominant disorder, which is in agreement with our findings.

OHCs function as cochlear amplifiers that enhance hearing thresholds by more than 40 dB, and loss of the amplifying function leads to 40–60 dB HI.[42,43] Because subjects with deleterious *MPZL2* variants displayed a 35–65 dB increase of hearing thresholds, the HI phenotype is compatible with predominant loss of OHCs. In addition, the remarkably good speech discrimination compared to the hearing thresholds and absence of OAEs in the affected individuals indicate abnormal OHC function.[44,45] Given the only moderate HI of the affected adult subjects of family W05-682 and subject I:2 of family W16-0451 at the age of about 40 years, we hypothesize that IHCs do not degenerate over time or that they do so very slowly.

MPZL2 (myelin protein zero-like 2), alternatively called EVA1 (epithelial V-like antigen 1), is a low-affinity adhesion molecule and a member of the immunoglobulin superfamily, more specifically of the family of immunoglobulin-like cell-adhesion molecules (Ig-CAMs).[32] Ig-CAMs form a large family of cell-surface molecules broadly expressed in, for example, epithelial and endothelial cells and in the nervous system. Ig-CAMs are known to interact directly with other classes of cell-surface molecules, such as cadherins, integrins, and tyrosine kinase receptors, and intracellularly they interact with cytoskeleton proteins such as actin and ankyrin (for review, see[46,47]).

The biological function of MPZL2 is likely to be related to its ability to mediate both homophilic and heterophilic cell-cell adhesions. In mice, *Mpzl2* is already expressed early in embryogenesis in various epithelial tissues as well as in adult tissues.[32,48] An adhesive function of *MPZL2* has been indicated in thymus histogenesis and T cell development,[32,33] placental morphogenesis,[49] the blood-cerebrospinal barrier,[50] lymphocyte adhesion to choroid plexus epithelial cells,[51] and mammary epithelial-cell differentiation.[48] Upregulation of *Mpzl2* in

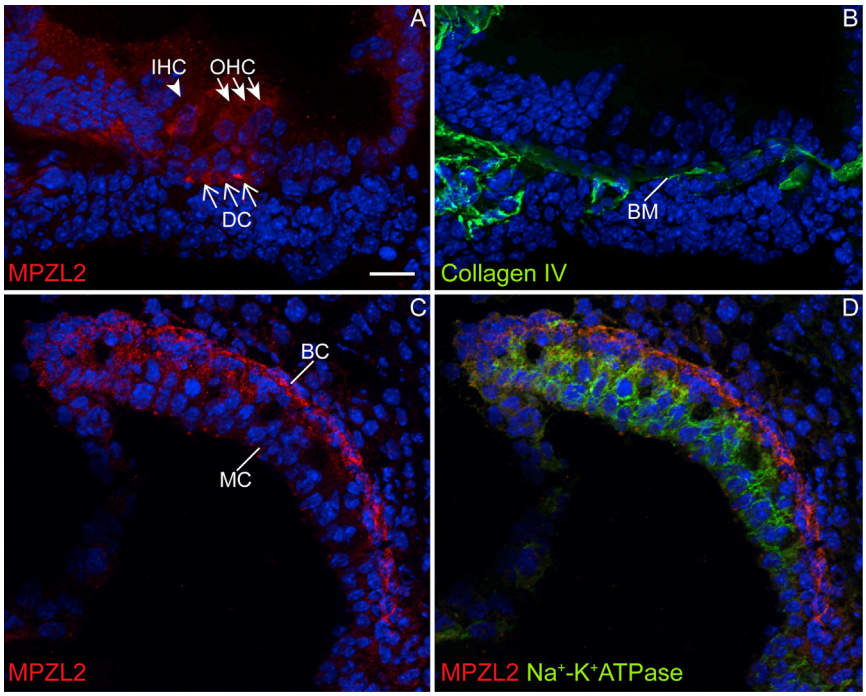

Figure 6. MPZL2 Displayed a Distinct Localization in the Cochlear Organ of Corti and Stria Vascularis at P4 in Wild-Type Mice

(A) MPZL2 (red) localizes in the organ of Corti in the basal region of Deiters cells (DCs) present below the three rows of outer hair cells (OHCs) and diffusely in inner hair cells (IHCs), OHCs, and DCs.

(B) In a serial section, collagen IV (green) immunostaining marked basement membranes, including the basilar membrane (BM), thereby indicating the localization of MPZL2 at the DC-BM contact region.

(C) In the stria vascularis, MPZL2 (red) immunostaining was observed predominantly in the basal cell (BC) region.

(D) Co-immunostaining of MPZL2 and Na^+-K^+ATPase (green), a marker for marginal cells (MCs), confirms immunostaining of MPZL2 (red) in the basal cells. Cell nuclei were stained with DAPI (blue). Arrowheads point to IHC, whitehead arrows to OHCs, and arrows to DCs. The scale bar (A–D) repsresents 20 μm.

spermatogenic cells of mice deficient in cell-adhesion molecule 1 further supports the cell-adhesive function.[52] Also, MPZL2 was demonstrated to function in the proliferation and tumorigenesis of glioblastoma-initiating cells[53] Despite these manifold indications of functional significance of MPZL2, no phenotypes other than HI were reported to be associated with MPZL2 deficiency.[53,54] This suggests that *MPZL2* function is essential only in the inner ear and that functional redundancy might well prohibit phenotypic effects in other tissues. This is similar to what is found for several other HI-associated genes, e.g., *KITLG* and *SMPX*.[7,55] However, more phenotypic effects might emerge under stress conditions, as is suggested by increased severity of experimentally induced autoimmune encephalomyelitis and white-matter tissue injury in MPZL2-deficient mice.[54]

In the developing and adult inner ear, several CAMs, belonging to different protein families, including the Ig-CAM superfamily, display a specific spatiotemporal pattern of expression, and several of these Ig-CAMs are critical for hearing and/or balance in both mice and humans.[56–63] The Ig-CAMs nectin-1 and -3, for example, are critical for establishing the checkerboard-like organization of hair cells and supporting cells in the cochlea.[64] The abnormal organization of DCs and OHCs, and their loss in *Mpzl2*-mutant mice at 12 weeks of age indicates that MPZL2 is essential for maintenance of the DC-OHC organization and integrity. A role in maintenance is supported by the moderate transcript levels of MPZL2 in adult human cochleae.[22]

Although no structural abnormalities were detected in cochleae of *Mpzl2* mutants at P4, MPZL2 is likely to function in prenatal cochlear development as well, in both mice and humans, as indicated by the finding that transcription of the gene was demonstrated in human embryos at 8 weeks of gestation and in mouse developing hair cells and their surrounding cells from embryonic day 16 (E16) to P16.[65] (See also the SHIELD database.) From the present study it is unclear whether *MPZL2*-associated HI is congenital or has an early-childhood onset. The fact that speech language development was disturbed in a number of cases indicates that onset of HI was prelingual in these individuals. If HI was congenital in the cases with prelingual HI, thresholds were below 35 dB HL because two of three individuals with prelingual HI passed a neonatal hearing screening. These tests are calibrated to pick up HI of more than 35 dB HL.[66]

We found MPZL2 to be a CAM that is present specifically at the base of DCs where they contact the basilar membrane. DCs develop a narrow infranuclear region that ends in feet-like junctions with the basal membrane.[67] The stripe-shaped signal in DCs in MPZL2 immunohistochemistry might represent the developing feet-like structures. It is tempting to speculate that MPZL2 is involved in the morphogenesis and/or maintenance of the characteristic structure of DCs by anchoring the actin-rich cytoskeletal core of the feet-like structures or the surrounding microtubules to the basilar membrane.[67] The relatively weak MPZL2 signal in immunohistochemistry at P4 in OHCs, IHCs, and the cytoplasm of DCs suggests that MPLZ2 (transiently) functions in homophilic or heterophilic cellular junctions of these cells and that absence of these junctions in *Mpzl2*-mutant mice might contribute to the disorganization and degeneration of the organ of Corti.

Although not much is known about the adhesive function of MPZL2 at the molecular level, some hints toward molecular interactions have been obtained. A co-association of MPZL2 and CLCA2 with tight junction protein ZO-1 has been described.[48] ZO-1 is an adaptor protein that functions in the coupling of TJs and adherens junctions (AJs) to the cytoskeleton.[68] Also, ZO-1 binds directly to occludin *in vitro*.[62] Interestingly, an association of MPZL2 and occludin has been observed in a high-throughput human protein interaction study.[69] Occludin is a tight-junction (TJ) protein essential for functional integrity of the reticular lamina of the organ of Corti.[60] The organ of Corti of $Occ^{-/-}$ mice degenerates, starting in the OHC region. Because of these associations and the defects in the organ of Corti in *Mpzl2*-mutant mice, it is tempting to speculate that MPZL2 is essential for (functional) integrity of cell junctions in the reticular lamina, especially in the OHC region, and thereby for ion homeostasis in the cochlea. The associations of MPZL2 with TJ and AJ proteins and their co-function in the cochlea have to be validated with other protein-interaction assays, as well as co-localization assays in the inner ear. The latter assays were impaired by the failure of antibodies to detect MPZL2 in the experimental conditions to be used in immunofluorescence of adult cochleae.

Recently, it was demonstrated that MPZL2 can activate the NF-κB signaling pathway, most likely by binding TRAF2, for which a consensus binding site is present in the cytoplasmic domain of MPLZ2.[53] This pathway was indicated to be protective for hair cell loss by environmental factors such as noise and aminoglycosides.[70,71] Therefore, defects of MPZL2 might lead to an increased sensitivity to noise and other environmental cues.

Although MPZL2 was detected in the basal cell layer of the developing stria vascularis, no gross histological abnormalities were observed in this region of the cochlea in *Mpzl2*-mutant mice, either at the age of 4 days or at 12 weeks of age. However, this does not fully exclude functional defects. A mild loss of spiral ganglion neurons was observed in the basal turn of the cochlea of *Mpzl2* mutants; this loss might have been secondary to hair-cell loss.

In conclusion, we demonstrated that MPZL2 is essential for normal cochlear function in humans and mice. In the latter species, defects of MPZL2 resulted in OHC and DC disorganization that is likely to interfere with mechanical and other functional properties of that region of the cochlea and ultimately in a loss of integrity of the organ of Corti. Humans affected by biallelic truncating *MPZL2* variants displayed slowly progressive NSHI, which is important in (genetic) counseling of subjects and their families.

Supplemental Data

Supplemental Data include Supplemental Methods, 13 figures, and seven tables and can be found with this article online at https://doi.org/10.1016/j.ajhg.2018.05.011.

Acknowledgments

We are grateful to the participating patients and their families. We thank Jeroen van Reeuwijk for discussions. We also acknowledge the experimental contributions of L. Hetterschijt, S. van der Velde-Visser, and E. de Vrieze and the technical assistance of the histology facilities (Centro Nacional de Biotecnología, Consejo Superior de Investigaciones Científicas [CSIC], and the Center for Biomedical Network Research on Rare Diseases [CIBERER]) and of the Non-invasive Neurofunctional Evaluation and Genomics facilities (IIBm, CSIC-UAM [Universidad Autónoma de Madrid], and CIBERER). This work was supported by a grant from the Heinsius Houbolt Foundation (to H.K., R.J.E.P., and H.P.M.K.) and partially by grants from the Spanish Ministry of Economy and Competitiveness and the European Regional Development Fund (Fonds Européen de Développement Économique et Régional, [FEDER]: SAF2014-53979-R) and from FEDER, CIBERER, and Instituto de Salud Carlos III (ISCIII) (to I.V.N.), and a grant from ISCIII to I.d.C. (PI14/01162; Plan Estatal de I+D+I 2013-2016, with co-funding from the European Regional Development Fund). S.M., A.M.C., and E.G.R. hold CIBERER ISCIII researcher contracts.

Declaration of Interests

The authors declare no competing interests.

Consortia

The DOOFNL consortium consists of M.F. van Dooren, H.H.W. de Gier, E.H. Hoefsloot, M.P. van der Schroeff, S.G. Kant, L.J.C. Rotteveel, S.G.M. Frints, J.R. Hof, R.J. Stokroos, E.K. Vanhoutte, R.J.C. Admiraal, I. Feenstra, H. Kremer, H.P.M. Kunst, R.J.E. Pennings, H.G. Yntema, A.J. van Essen, R.H. Free, and J.S. Klein-Wassink.

Received: October 5, 2017
Accepted: May 25, 2018
Published: June 28, 2018

Web Resources

Alamut Visual, http://www.interactive-biosoftware.com/alamut-visual/
BioGRID, https://thebiogrid.org
ExAC Browser, http://exac.broadinstitute.org/
Genome Diagnostics Radboudumc, https://www.radboudumc.nl/en/patientenzorg/onderzoeken/exome-sequencing-diagnostics/exomepanelspreviousversions/hearing-impairment
GnomAD Browser, http://gnomad.broadinstitute.org/
Hereditary Hearing Loss, http://hereditaryhearingloss.org/
HomozygosityMapper, http://www.homozygositymapper.org/
IMPC, http://www.mousephenotype.org/
Marshfield Genetic Maps, http://research.marshfieldclinic.org/genetics/GeneticResearch/compMaps.asp
MGI, http://www.informatics.jax.org/
Mutation Taster, http://www.mutationtaster.org/
Ocular Tissue Database, https://genome.uiowa.edu/otdb/
Oligo Primer Analysis Software, http://www.oligo.net/
OMIM, http://www.omim.org/
OMIM Phenotypic Series, http://www.omim.org/phenotypicSeriesTitle/all

Primer3Plus, http://www.bioinformatics.nl/cgi-bin/primer3plus/primer3plus.cgi
SMART, http://smart.embl-heidelberg.de/
STRING, https://string-db.org
UCSC Genome Browser, https://genome.ucsc.edu

References

1. Sommen, M., Schrauwen, I., Vandeweyer, G., Boeckx, N., Corneveaux, J.J., van den Ende, J., Boudewyns, A., De Leenheer, E., Janssens, S., Claes, K., et al. (2016). DNA diagnostics of hereditary hearing loss: A targeted resequencing approach combined with a mutation classification system. Hum. Mutat. *37*, 812–819.
2. Yan, D., Tekin, D., Bademci, G., Foster, J., 2nd, Cengiz, F.B., Kannan-Sundhari, A., Guo, S., Mittal, R., Zou, B., Grati, M., et al. (2016). Spectrum of DNA variants for non-syndromic deafness in a large cohort from multiple continents. Hum. Genet. *135*, 953–961.
3. Sloan-Heggen, C.M., Bierer, A.O., Shearer, A.E., Kolbe, D.L., Nishimura, C.J., Frees, K.L., Ephraim, S.S., Shibata, S.B., Booth, K.T., Campbell, C.A., et al. (2016). Comprehensive genetic testing in the clinical evaluation of 1119 patients with hearing loss. Hum. Genet. *135*, 441–450.
4. Shearer, A.E., Black-Ziegelbein, E.A., Hildebrand, M.S., Eppsteiner, R.W., Ravi, H., Joshi, S., Guiffre, A.C., Sloan, C.M., Happe, S., Howard, S.D., et al. (2013). Advancing genetic testing for deafness with genomic technology. J. Med. Genet. *50*, 627–634.
5. Atik, T., Onay, H., Aykut, A., Bademci, G., Kirazli, T., Tekin, M., and Ozkinay, F. (2015). Comprehensive analysis of deafness genes in families with autosomal-recessive nonsyndromic hearing loss. PLoS ONE *10*, e0142154.
6. Zazo Seco, C., Wesdorp, M., Feenstra, I., Pfundt, R., Hehir-Kwa, J.Y., Lelieveld, S.H., Castelein, S., Gilissen, C., de Wijs, I.J., Admiraal, R.J., et al. (2017). The diagnostic yield of whole-exome sequencing targeting a gene panel for hearing impairment in the Netherlands. Eur. J. Hum. Genet. *25*, 308–314.
7. Zazo Seco, C., Serrão de Castro, L., van Nierop, J.W., Morín, M., Jhangiani, S., Verver, E.J., Schraders, M., Maiwald, N., Wesdorp, M., Venselaar, H., et al.; Baylor-Hopkins Center for Mendelian Genomics (2015). Allelic mutations of *KITLG*, encoding KIT ligand, cause asymmetric and unilateral hearing loss and Waardenburg syndrome type 2. Am. J. Hum. Genet. *97*, 647–660.
8. Zazo Seco, C., Castells-Nobau, A., Joo, S.H., Schraders, M., Foo, J.N., van der Voet, M., Velan, S.S., Nijhof, B., Oostrik, J., de Vrieze, E., et al. (2017). A homozygous FITM2 mutation causes a deafness-dystonia syndrome with motor regression and signs of ichthyosis and sensory neuropathy. Dis. Model. Mech. *10*, 105–118.
9. Garabatos, N., Blanco, J., Fandos, C., Lopez, E., Santamaria, P., Ruiz, A., Perez-Vidakovics, M.L., Benveniste, P., Galkin, O., Zuñiga-Pflucker, J.C., and Serra, P. (2014). A monoclonal antibody against the extracellular domain of mouse and human epithelial V-like antigen 1 reveals a restricted expression pattern among CD4- CD8- thymocytes. Monoclon. Antib. Immunodiagn. Immunother. *33*, 305–311.
10. Mazzoli, M., Van Camp, G., Newton, V., Giarbini, N., Declau, F., and Parving, A. (2003). Recommendations for the description of genetic and audiological data for families with nonsyndromic hereditary hearing impairment. Audiol. Med. *1*, 148–150.
11. Huygen, P.L.M., Pennings, R.J.E., and Cremers, C.W.R.J. (2003). Characterizing and distinguishing progressive phenotypes in nonsyndromic autosomal dominant hearing impairment. Audiol. Med. *1*, 37–46.
12. Bosman, A.J., and Smoorenburg, G.F. (1995). Intelligibility of Dutch CVC syllables and sentences for listeners with normal hearing and with three types of hearing impairment. Audiology *34*, 260–284.
13. Wallis, Y., Payne, S., McAnulty, C., Bodmer, D., Sistermans, E., Robertson, K., Moore, D., Abbs, S., Deans, Z., and Devereau, A. (2013). Practice guidelines for the evaluation of pathogenicity and the reporting of sequence variants in clinical molecular genetics (ACGS and VGKL).
14. Seelow, D., Schuelke, M., Hildebrandt, F., and Nürnberg, P. (2009). HomozygosityMapper—An interactive approach to homozygosity mapping. Nucleic Acids Res. *37*, W593–W599.
15. Pfundt, R., Del Rosario, M., Vissers, L.E.L.M., Kwint, M.P., Janssen, I.M., de Leeuw, N., Yntema, H.G., Nelen, M.R., Lugtenberg, D., Kamsteeg, E.J., et al. (2017). Detection of clinically relevant copy-number variants by exome sequencing in a large cohort of genetic disorders. Genet. Med. *19*, 667–675.
16. Krumm, N., Sudmant, P.H., Ko, A., O'Roak, B.J., Malig, M., Coe, B.P., NHLBI Exome Sequencing Project,, Quinlan, A.R., Nickerson, D.A., and Eichler, E.E. (2012). Copy number variation detection and genotyping from exome sequence data. Genome Res. *22*, 1525–1532.
17. Luijendijk, M.W., van de Pol, T.J., van Duijnhoven, G., den Hollander, A.I., ten Caat, J., van Limpt, V., Brunner, H.G., Kremer, H., and Cremers, F.P. (2003). Cloning, characterization, and mRNA expression analysis of novel human fetal cochlear cDNAs. Genomics *82*, 480–490.
18. Pfaffl, M.W. (2001). A new mathematical model for relative quantification in real-time RT-PCR. Nucleic Acids Res. *29*, e45.
19. Cediel, R., Riquelme, R., Contreras, J., Díaz, A., and Varela-Nieto, I. (2006). Sensorineural hearing loss in insulin-like growth factor I-null mice: A new model of human deafness. Eur. J. Neurosci. *23*, 587–590.
20. Murillo-Cuesta, S., Rodríguez-de la Rosa, L., Contreras, J., Celaya, A.M., Camarero, G., Rivera, T., and Varela-Nieto, I. (2015). Transforming growth factor β1 inhibition protects from noise-induced hearing loss. Front. Aging Neurosci. *7*, 32.
21. Skvorak, A.B., Weng, Z., Yee, A.J., Robertson, N.G., and Morton, C.C. (1999). Human cochlear expressed sequence tags provide insight into cochlear gene expression and identify candidate genes for deafness. Hum. Mol. Genet. *8*, 439–452.
22. Schrauwen, I., Hasin-Brumshtein, Y., Corneveaux, J.J., Ohmen, J., White, C., Allen, A.N., Lusis, A.J., Van Camp, G., Huentelman, M.J., and Friedman, R.A. (2016). A comprehensive catalogue of the coding and non-coding transcripts of the human inner ear. Hear. Res. *333*, 266–274.
23. Hodoğlugil, U., and Mahley, R.W. (2012). Turkish population structure and genetic ancestry reveal relatedness among Eurasian populations. Ann. Hum. Genet. *76*, 128–141.
24. Brownell, W.E. (1990). Outer hair cell electromotility and otoacoustic emissions. Ear Hear. *11*, 82–92.
25. Su, Y., Brooks, D.G., Li, L., Lepercq, J., Trofatter, J.A., Ravetch, J.V., and Lebo, R.V. (1993). Myelin protein zero gene mutated in Charcot-Marie-tooth type 1B patients. Proc. Natl. Acad. Sci. USA *90*, 10856–10860.
26. Mastaglia, F.L., Nowak, K.J., Stell, R., Phillips, B.A., Edmondston, J.E., Dorosz, S.M., Wilton, S.D., Hallmayer, J., Kakulas,

B.A., and Laing, N.G. (1999). Novel mutation in the myelin protein zero gene in a family with intermediate hereditary motor and sensory neuropathy. J. Neurol. Neurosurg. Psychiatry *67*, 174–179.
27. Marrosu, M.G., Vaccargiu, S., Marrosu, G., Vannelli, A., Cianchetti, C., and Muntoni, F. (1998). Charcot-Marie-Tooth disease type 2 associated with mutation of the myelin protein zero gene. Neurology *50*, 1397–1401.
28. Chapon, F., Latour, P., Diraison, P., Schaeffer, S., and Vandenberghe, A. (1999). Axonal phenotype of Charcot-Marie-Tooth disease associated with a mutation in the myelin protein zero gene. J. Neurol. Neurosurg. Psychiatry *66*, 779–782.
29. Hayasaka, K., Himoro, M., Sawaishi, Y., Nanao, K., Takahashi, T., Takada, G., Nicholson, G.A., Ouvrier, R.A., and Tachi, N. (1993). De novo mutation of the myelin P0 gene in Dejerine-Sottas disease (hereditary motor and sensory neuropathy type III). Nat. Genet. *5*, 266–268.
30. Warner, L.E., Hilz, M.J., Appel, S.H., Killian, J.M., Kolodry, E.H., Karpati, G., Carpenter, S., Watters, G.V., Wheeler, C., Witt, D., et al. (1996). Clinical phenotypes of different MPZ (P0) mutations may include Charcot-Marie-Tooth type 1B, Dejerine-Sottas, and congenital hypomyelination. Neuron *17*, 451–460.
31. Planté-Bordeneuve, V., Guiochon-Mantel, A., Lacroix, C., Lapresle, J., and Said, G. (1999). The Roussy-Lévy family: From the original description to the gene. Ann. Neurol. *46*, 770–773.
32. Guttinger, M., Sutti, F., Panigada, M., Porcellini, S., Merati, B., Mariani, M., Teesalu, T., Consalez, G.G., and Grassi, F. (1998). Epithelial V-like antigen (EVA), a novel member of the immunoglobulin superfamily, expressed in embryonic epithelia with a potential role as homotypic adhesion molecule in thymus histogenesis. J. Cell Biol. *141*, 1061–1071.
33. DeMonte, L., Porcellini, S., Tafi, E., Sheridan, J., Gordon, J., Depreter, M., Blair, N., Panigada, M., Sanvito, F., Merati, B., et al. (2007). EVA regulates thymic stromal organisation and early thymocyte development. Biochem. Biophys. Res. Commun. *356*, 334–340.
34. Iacovelli, S., Iosue, I., Di Cesare, S., and Guttinger, M. (2009). Lymphoid EVA1 expression is required for DN1-DN3 thymocytes transition. PLoS ONE *4*, e7586.
35. Wagner, A.H., Anand, V.N., Wang, W.H., Chatterton, J.E., Sun, D., Shepard, A.R., Jacobson, N., Pang, I.H., Deluca, A.P., Casavant, T.L., et al. (2013). Exon-level expression profiling of ocular tissues. Exp. Eye Res. *111*, 105–111.
36. Fuentes-Santamaría, V., Alvarado, J.C., Rodríguez-de la Rosa, L., Murillo-Cuesta, S., Contreras, J., Juiz, J.M., and Varela-Nieto, I. (2016). IGF-1 deficiency causes atrophic changes associated with upregulation of VGluT1 and downregulation of MEF2 transcription factors in the mouse cochlear nuclei. Brain Struct. Funct. *221*, 709–734.
37. Mann, Z.F., and Kelley, M.W. (2011). Development of tonotopy in the auditory periphery. Hear. Res. *276*, 2–15.
38. Alasti, F., Sanati, M.H., Behrouzifard, A.H., Sadeghi, A., de Brouwer, A.P., Kremer, H., Smith, R.J., and Van Camp, G. (2008). A novel TECTA mutation confirms the recognizable phenotype among autosomal recessive hearing impairment families. Int. J. Pediatr. Otorhinolaryngol. *72*, 249–255.
39. Behlouli, A., Bonnet, C., Abdi, S., Hasbellaoui, M., Boudjenah, F., Hardelin, J.P., Louha, M., Makrelouf, M., Ammar-Khodja, F., Zenati, A., and Petit, C. (2016). A novel biallelic splice site mutation of TECTA causes moderate to severe hearing impairment in an Algerian family. Int. J. Pediatr. Otorhinolaryngol. *87*, 28–33.
40. Lek, M., Karczewski, K.J., Minikel, E.V., Samocha, K.E., Banks, E., Fennell, T., O'Donnell-Luria, A.H., Ware, J.S., Hill, A.J., Cummings, B.B., et al.; Exome Aggregation Consortium (2016). Analysis of protein-coding genetic variation in 60,706 humans. Nature *536*, 285–291.
41. Quinodoz, M., Royer-Bertrand, B., Cisarova, K., Di Gioia, S.A., Superti-Furga, A., and Rivolta, C. (2017). DOMINO: Using machine learning to predict genes associated with dominant disorders. Am. J. Hum. Genet. *101*, 623–629.
42. Ryan, A., and Dallos, P. (1975). Effect of absence of cochlear outer hair cells on behavioural auditory threshold. Nature *253*, 44–46.
43. Liberman, M.C., Gao, J., He, D.Z., Wu, X., Jia, S., and Zuo, J. (2002). Prestin is required for electromotility of the outer hair cell and for the cochlear amplifier. Nature *419*, 300–304.
44. Dorn, P.A., Piskorski, P., Gorga, M.P., Neely, S.T., and Keefe, D.H. (1999). Predicting audiometric status from distortion product otoacoustic emissions using multivariate analyses. Ear Hear. *20*, 149–163.
45. Hoben, R., Easow, G., Pevzner, S., and Parker, M.A. (2017). Outer hair cell and auditory nerve function in speech recognition in quiet and in background noise. Front. Neurosci. *11*, 157.
46. Bombardelli, L., and Cavallaro, U. (2010). Immunoglobulin-like cell adhesion molecules: Novel signaling players in epithelial ovarian cancer. Int. J. Biochem. Cell Biol. *42*, 590–594.
47. Rougon, G., and Hobert, O. (2003). New insights into the diversity and function of neuronal immunoglobulin superfamily molecules. Annu. Rev. Neurosci. *26*, 207–238.
48. Ramena, G., Yin, Y., Yu, Y., Walia, V., and Elble, R.C. (2016). CLCA2 interactor EVA1 is required for mammary epithelial cell differentiation. PLoS ONE *11*, e0147489.
49. Teesalu, T., Grassi, F., and Guttinger, M. (1998). Expression pattern of the epithelial v-like antigen (Eva) transcript suggests a possible role in placental morphogenesis. Dev. Genet. *23*, 317–323.
50. Chatterjee, G., Carrithers, L.M., and Carrithers, M.D. (2008). Epithelial V-like antigen regulates permeability of the blood-CSF barrier. Biochem. Biophys. Res. Commun. *372*, 412–417.
51. Wojcik, E., Carrithers, L.M., and Carrithers, M.D. (2011). Characterization of epithelial V-like antigen in human choroid plexus epithelial cells: Potential role in CNS immune surveillance. Neurosci. Lett. *495*, 115–120.
52. Nakata, H., Wakayama, T., Adthapanyawanich, K., Nishiuchi, T., Murakami, Y., Takai, Y., and Iseki, S. (2012). Compensatory upregulation of myelin protein zero-like 2 expression in spermatogenic cells in cell adhesion molecule-1-deficient mice. Acta Histochem. Cytochem. *45*, 47–56.
53. Ohtsu, N., Nakatani, Y., Yamashita, D., Ohue, S., Ohnishi, T., and Kondo, T. (2016). Eva1 maintains the stem-like character of glioblastoma-initiating cells by activating the noncanonical NF-κB signaling pathway. Cancer Res. *76*, 171–181.
54. Wright, E., Rahgozar, K., Hallworth, N., Lanker, S., and Carrithers, M.D. (2013). Epithelial V-like antigen mediates efficacy of anti-alpha$_4$ integrin treatment in a mouse model of multiple sclerosis. PLoS ONE *8*, e70954.
55. Schraders, M., Haas, S.A., Weegerink, N.J., Oostrik, J., Hu, H., Hoefsloot, L.H., Kannan, S., Huygen, P.L., Pennings, R.J., Admiraal, R.J., et al. (2011). Next-generation sequencing

identifies mutations of SMPX, which encodes the small muscle protein, X-linked, as a cause of progressive hearing impairment. Am. J. Hum. Genet. *88*, 628–634.
56. Whitlon, D.S. (1993). E-cadherin in the mature and developing organ of Corti of the mouse. J. Neurocytol. *22*, 1030–1038.
57. Simonneau, L., Gallego, M., and Pujol, R. (2003). Comparative expression patterns of T-, N-, E-cadherins, beta-catenin, and polysialic acid neural cell adhesion molecule in rat cochlea during development: Implications for the nature of Kölliker's organ. J. Comp. Neurol. *459*, 113–126.
58. Nakano, Y., Kim, S.H., Kim, H.M., Sanneman, J.D., Zhang, Y., Smith, R.J., Marcus, D.C., Wangemann, P., Nessler, R.A., and Bánfi, B. (2009). A claudin-9-based ion permeability barrier is essential for hearing. PLoS Genet. *5*, e1000610.
59. Ben-Yosef, T., Belyantseva, I.A., Saunders, T.L., Hughes, E.D., Kawamoto, K., Van Itallie, C.M., Beyer, L.A., Halsey, K., Gardner, D.J., Wilcox, E.R., et al. (2003). Claudin 14 knockout mice, a model for autosomal recessive deafness DFNB29, are deaf due to cochlear hair cell degeneration. Hum. Mol. Genet. *12*, 2049–2061.
60. Kitajiri, S., Katsuno, T., Sasaki, H., Ito, J., Furuse, M., and Tsukita, S. (2014). Deafness in occludin-deficient mice with dislocation of tricellulin and progressive apoptosis of the hair cells. Biol. Open *3*, 759–766.
61. Kamitani, T., Sakaguchi, H., Tamura, A., Miyashita, T., Yamazaki, Y., Tokumasu, R., Inamoto, R., Matsubara, A., Mori, N., Hisa, Y., and Tsukita, S. (2015). Deletion of tricellulin causes progressive hearing loss associated with degeneration of cochlear hair cells. Sci. Rep. *5*, 18402.
62. Riazuddin, S., Ahmed, Z.M., Fanning, A.S., Lagziel, A., Kitajiri, S., Ramzan, K., Khan, S.N., Chattaraj, P., Friedman, P.L., Anderson, J.M., et al. (2006). Tricellulin is a tight-junction protein necessary for hearing. Am. J. Hum. Genet. *79*, 1040–1051.
63. Wilcox, E.R., Burton, Q.L., Naz, S., Riazuddin, S., Smith, T.N., Ploplis, B., Belyantseva, I., Ben-Yosef, T., Liburd, N.A., Morell, R.J., et al. (2001). Mutations in the gene encoding tight junction claudin-14 cause autosomal recessive deafness DFNB29. Cell *104*, 165–172.
64. Togashi, H., Kominami, K., Waseda, M., Komura, H., Miyoshi, J., Takeichi, M., and Takai, Y. (2011). Nectins establish a checkerboard-like cellular pattern in the auditory epithelium. Science *333*, 1144–1147.
65. Scheffer, D.I., Shen, J., Corey, D.P., and Chen, Z.Y. (2015). Gene expression by mouse inner ear hair cells during development. J. Neurosci. *35*, 6366–6380.
66. van der Ploeg, C.P., Uilenburg, N.N., Kauffman-de Boer, M.A., Oudesluys-Murphy, A.M., and Verkerk, P.H. (2012). Newborn hearing screening in youth health care in the Netherlands: National results of implementation and follow-up. Int. J. Audiol. *51*, 584–590.
67. Parsa, A., Webster, P., and Kalinec, F. (2012). Deiters cells tread a narrow path—The Deiters cells-basilar membrane junction. Hear. Res. *290*, 13–20.
68. González-Mariscal, L., Betanzos, A., and Avila-Flores, A. (2000). MAGUK proteins: Structure and role in the tight junction. Semin. Cell Dev. Biol. *11*, 315–324.
69. Huttlin, E.L., Ting, L., Bruckner, R.J., Gebreab, F., Gygi, M.P., Szpyt, J., Tam, S., Zarraga, G., Colby, G., Baltier, K., et al. (2015). The BioPlex Network: A systematic exploration of the human interactome. Cell *162*, 425–440.
70. Tamura, A., Matsunobu, T., Tamura, R., Kawauchi, S., Sato, S., and Shiotani, A. (2016). Photobiomodulation rescues the cochlea from noise-induced hearing loss via upregulating nuclear factor κB expression in rats. Brain Res. *1646*, 467–474.
71. Dinh, C.T., Bas, E., Chan, S.S., Dinh, J.N., Vu, L., and Van De Water, T.R. (2011). Dexamethasone treatment of tumor necrosis factor-alpha challenged organ of Corti explants activates nuclear factor kappa B signaling that induces changes in gene expression that favor hair cell survival. Neuroscience *188*, 157–167.

The American Journal of Human Genetics, Volume *103*

Supplemental Data

MPZL2, Encoding the Epithelial Junctional Protein Myelin Protein Zero-like 2, Is Essential for Hearing in Man and Mouse

Mieke Wesdorp, Silvia Murillo-Cuesta, Theo Peters, Adelaida M. Celaya, Anne Oonk, Margit Schraders, Jaap Oostrik, Elena Gomez-Rosas, Andy J. Beynon, Bas P. Hartel, Kees Okkersen, Hans J.P.M. Koenen, Jack Weeda, Stefan Lelieveld, Nicol C. Voermans, Irma Joosten, Carel B. Hoyng, Peter Lichtner, Henricus P.M. Kunst, Ilse Feenstra, Suzanne E. de Bruijn, DOOFNL Consortium, Ronald J.C. Admiraal, Helger G. Yntema, Erwin van Wijk, Ignacio del Castillo, Pau Serra, Isabel Varela-Nieto, Ronald J.E. Pennings, and Hannie Kremer

Supplemental Figures

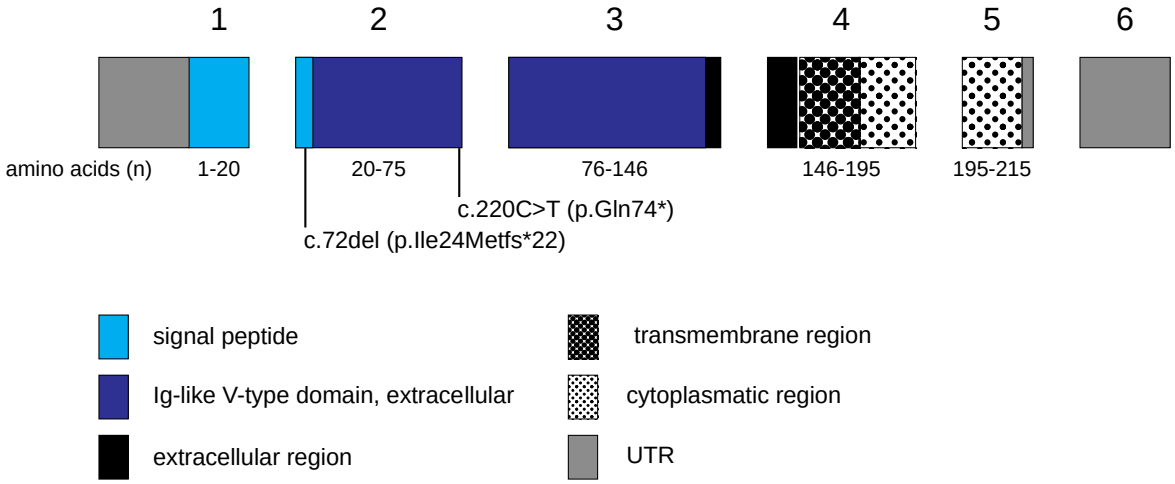

Figure S1. Exonic and protein structure of *MPZL2*/MPZL2 and pathogenic variants
Schematic representation of the genomic structure and the encoded protein domains of *MPZL2* (NM_005797.3). Identified pathogenic variants are indicated. Protein domain predictions were extracted from the SMART domain database (http://smart.embl-heidelberg.de/), using the *PFAM domains* setting.

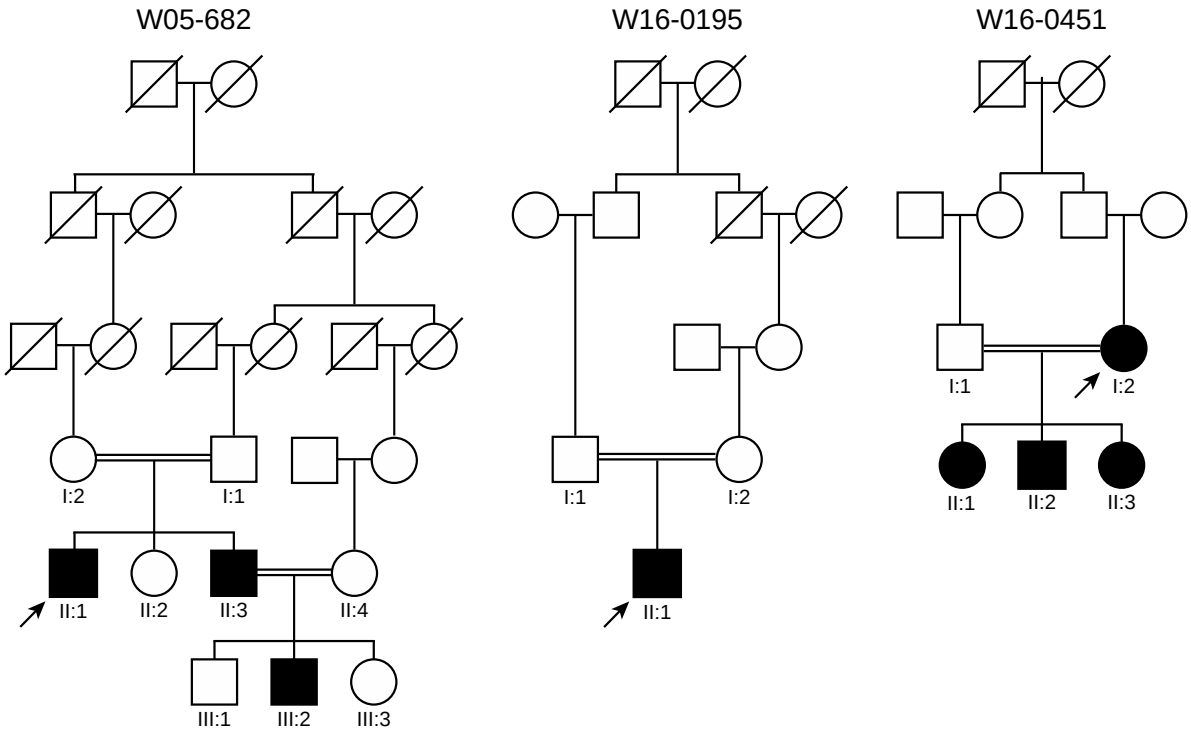

Figure S2. Extended pedigrees of families affected by *MPZL2* variants
Index cases are marked by arrows. Double lines indicate consanguinity.

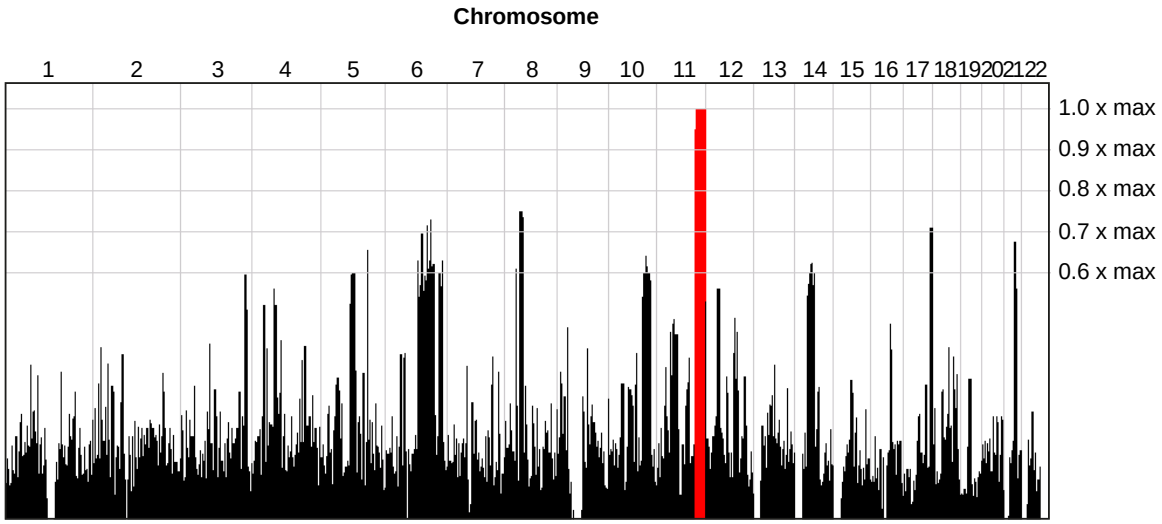

Figure S3. Homozygosity mapping in family W05-682

Graphical representation of the genome-wide homozygosity scores in family W05-682, produced by HomozygosityMapper.[1] Homozygosity mapping was performed by genotyping of subjects II:1 and II:3 of family W05-682 with the Affymetrix mapping 250K SNP array, and subsequent genotype calling with Genotype Console software (Santa Clara, CA, USA) and homozygosity mapping with the online tool HomozygosityMapper (http://www.homozygositymapper.org/). This revealed a single homozygous region of 23.8 Mb on chromosome 11q23.1-q25, flanked by rs4936310 and rs10458997. There were no other significant regions of homozygosity.

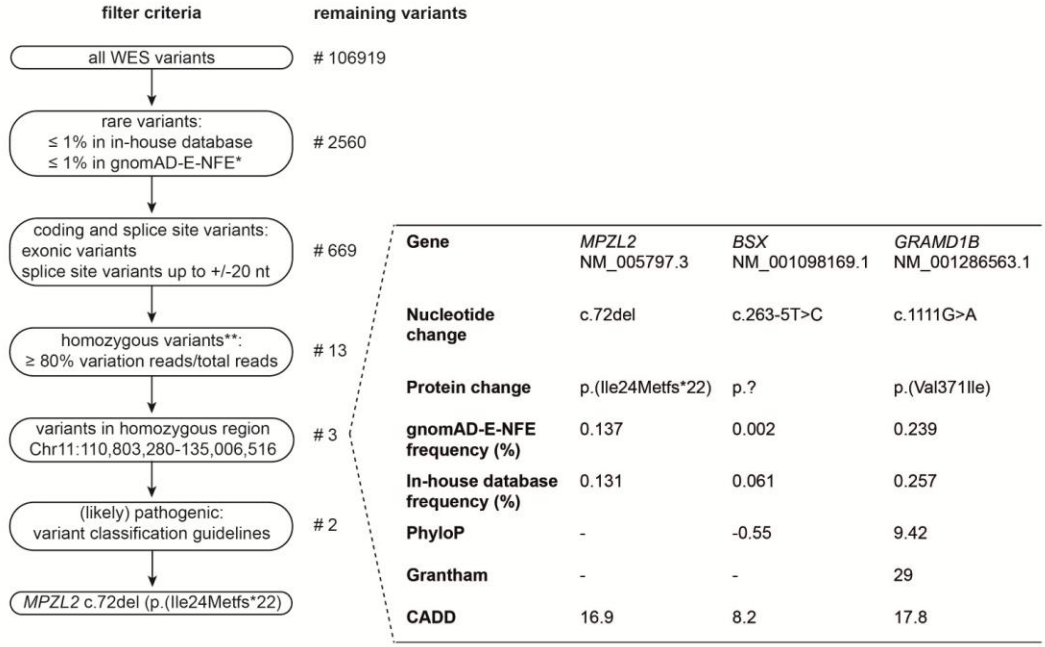

Figure S4. Filtering of WES variants in the largest homozygous region on chromosome 11q23.1-q25 of family W05-682

Criteria of variant filtering and resulting number of variants of WES data for the index case (II:1) of family W05-682. The in-house database contains WES data of ~15,000 individuals, the vast majority of Dutch origin, healthy or affected by different diseases (including 810 subjects with HI). *Minor allele frequencies in the exome data of the the non-Finnish European population in the gnomAD database. **Chromosome X was excluded from the analysis. All 13 homozygous variants are listed in Table S3.

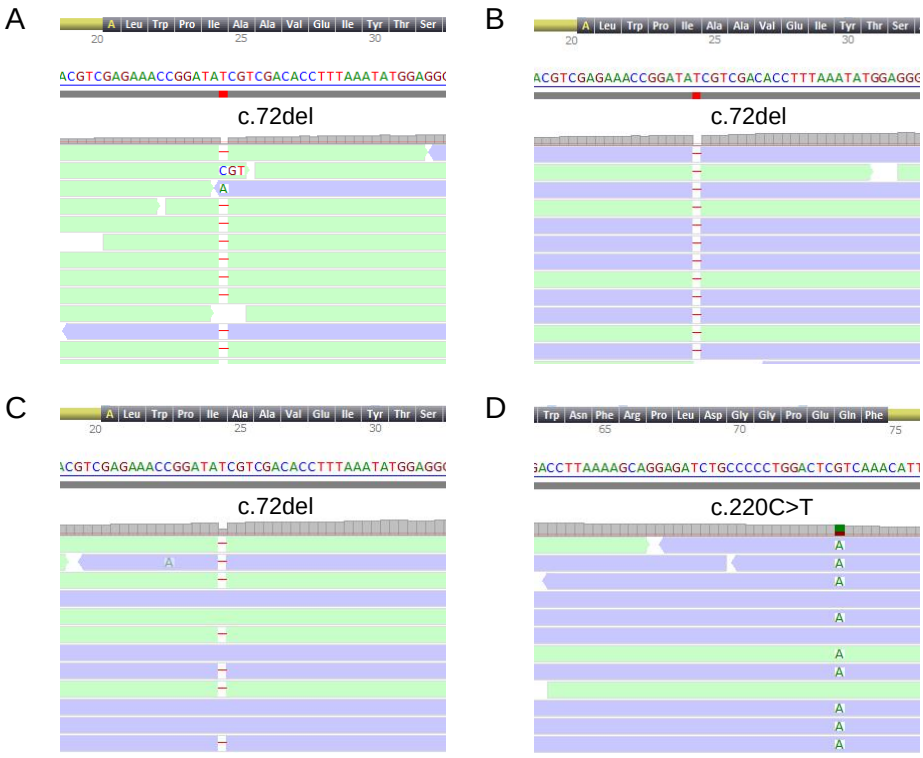

Figure S5. Sequences of *MPZL2* c.72del and c.220C>T

Analysis of the WES paired-reads demonstrated a homozygous point deletion, *MPZL2* c.72del, in the index cases of families W05-682 (**A**) and W16-0195 (**B**). In the index case of family W16-0451, WES revealed the c.72del variant heterozygously (**C**) and the heterozygous missense variant *MPZL2* c.220C>T (**D**). NM_005797.3 was used as reference sequence. Figures were obtained using Alamut Visual (Interactive Biosoftware, Rouen, France).

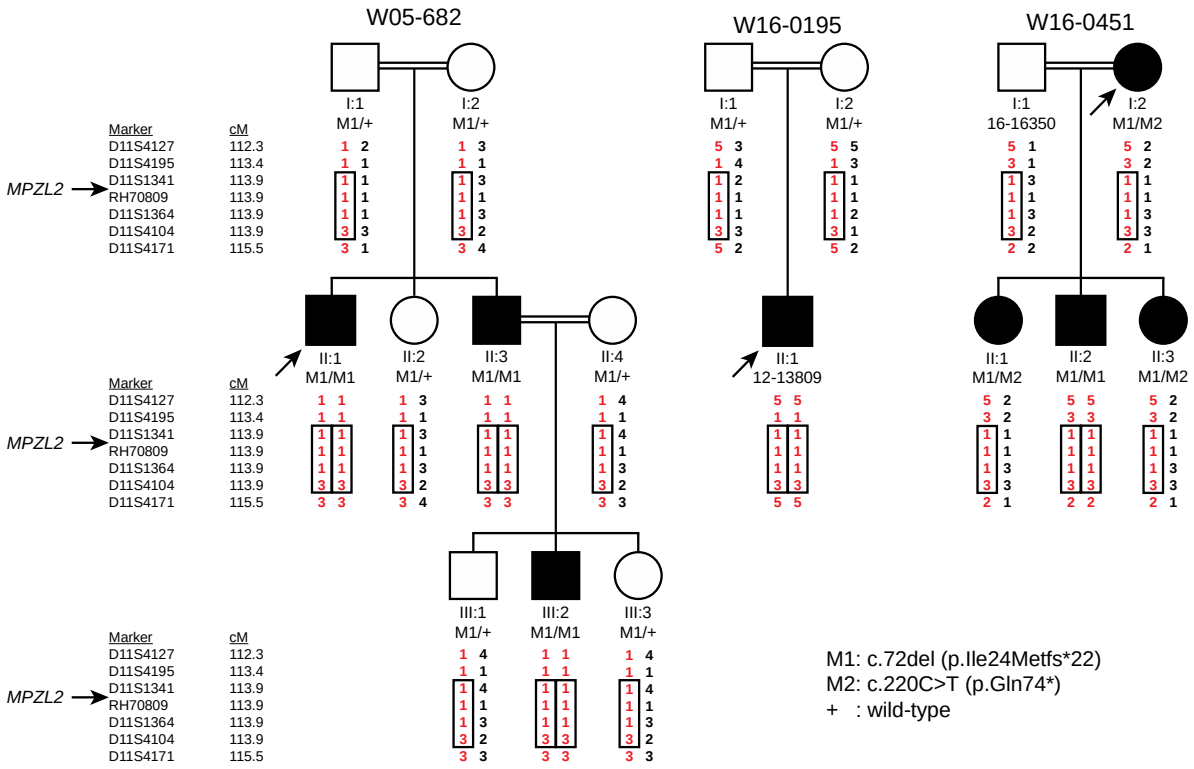

Figure S6. Haplotype analysis of the genomic region harboring *MPZL2*

MPZL2 haplotypes were determined by genotyping VNTR-markers in families W05-682, W16-0195 and W16-0451. All c.72del *MPZL2* alleles (depicted in red) shared a haplotype of at least 0.5 Mb, delimited by markers D11S1341 and D11S4104 (boxed), suggesting that it is derived from a common ancestor. Index cases are marked by arrows.

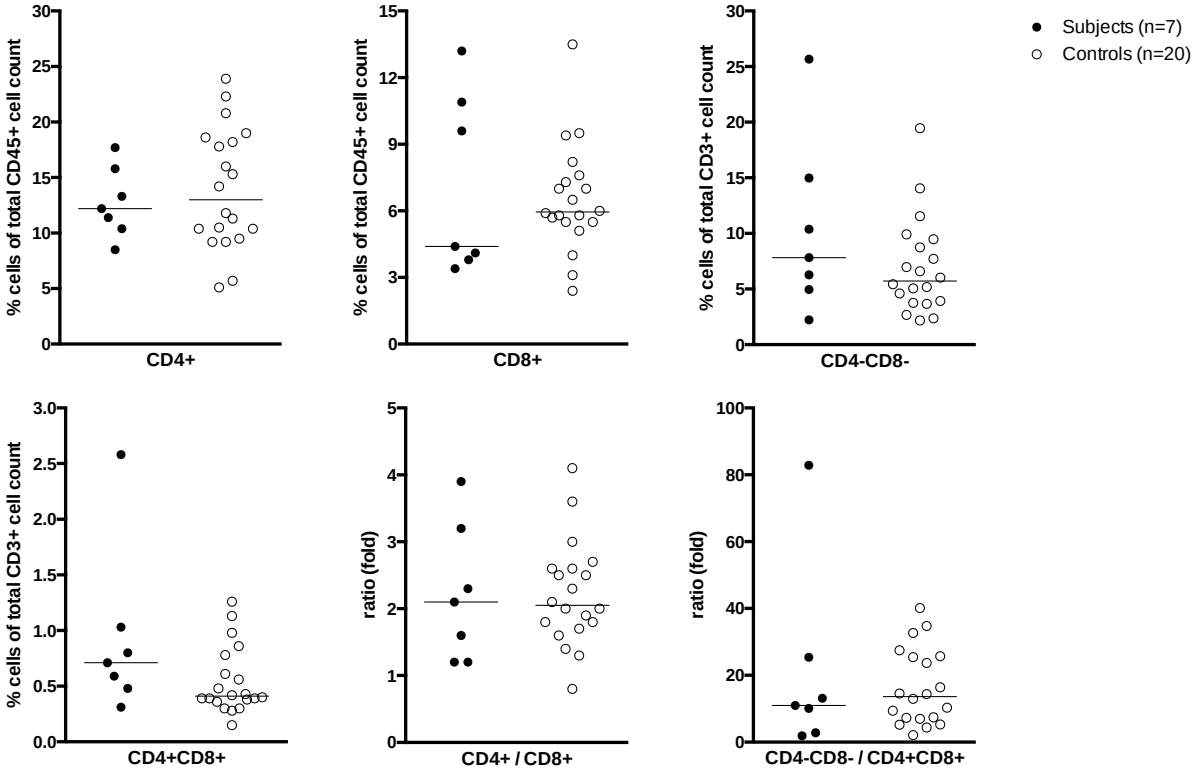

Figure S7. CD4 and CD8 expression on human T cells

The number of CD4 and CD8 expressing human T cells was analyzed in affected individuals (family W05-682, II:1, II:3, III:2; family W16-0195, II:1; family W16-0451, I:2, II:2, II:3), as described in detail before.[4] In brief, peripheral blood was collected in EDTA-tubes, and after red cell lysis, leucocytes were stained with fluorochrome labelled antibodies against CD3 (UCHT-1 pe), CD4 (13B8.2 pacific blue), CD8 (B9.11 APC-AF750) and CD45 (J33 Krome Orange) (all from Beckman Coulter, Brea, USA). Data was acquired on a Navios flow cytometer (Beckman Coulter) and analyzed using Kaluza® software version 1.3 (Beckman Coulter). Presented cell counts are a percentage of total CD45+ cells (CD4+ and CD8+), a percentage of total CD3+ cells (CD4-CD8- and CD4+CD8+) or a fold ratio. Data of 20 healthy individuals was used as control. Individual and median cell counts and ratios are shown. Numbers of cells and ratios are comparable between subjects and controls, indicating normal CD4 and CD8 T cell counts. Mann-Whitney U tests did not demonstrate significant differences.

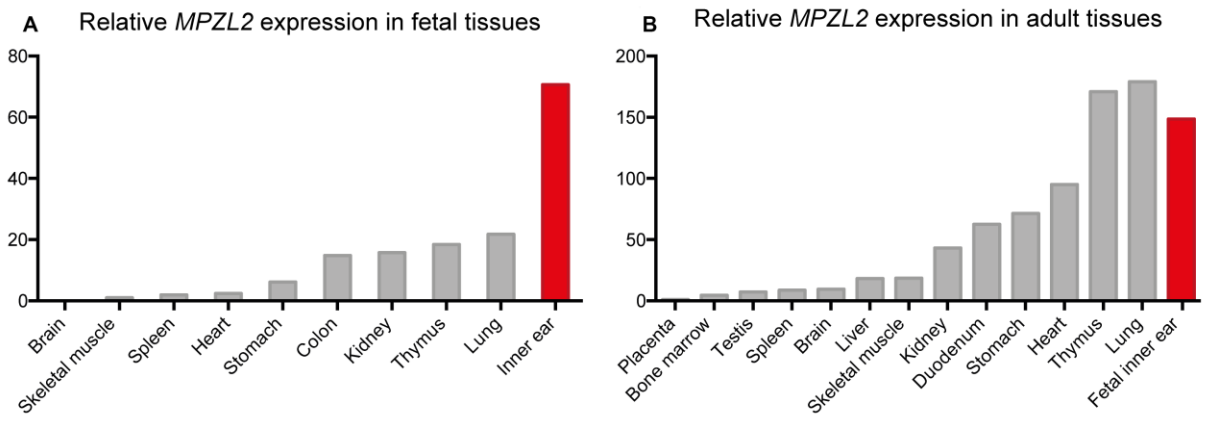

Figure S8. *MPZL2* expression profile in human tissues

Relative *MPZL2* mRNA levels as determined by RT-qPCR in human fetal **(A)** and adult **(B)** tissues. The relative expression values were determined by the delta-delta Ct method with *GUSB* as a reference gene.[2] Expression levels are relative to those in skeletal muscle (**A)** and placenta (**B**), which displayed the lowest detectable *MPZL2* expression of tested fetal and adult tissues, respectively. In fetal brain, no expression of *MPZL2* could be detected. The experiment was performed twice.

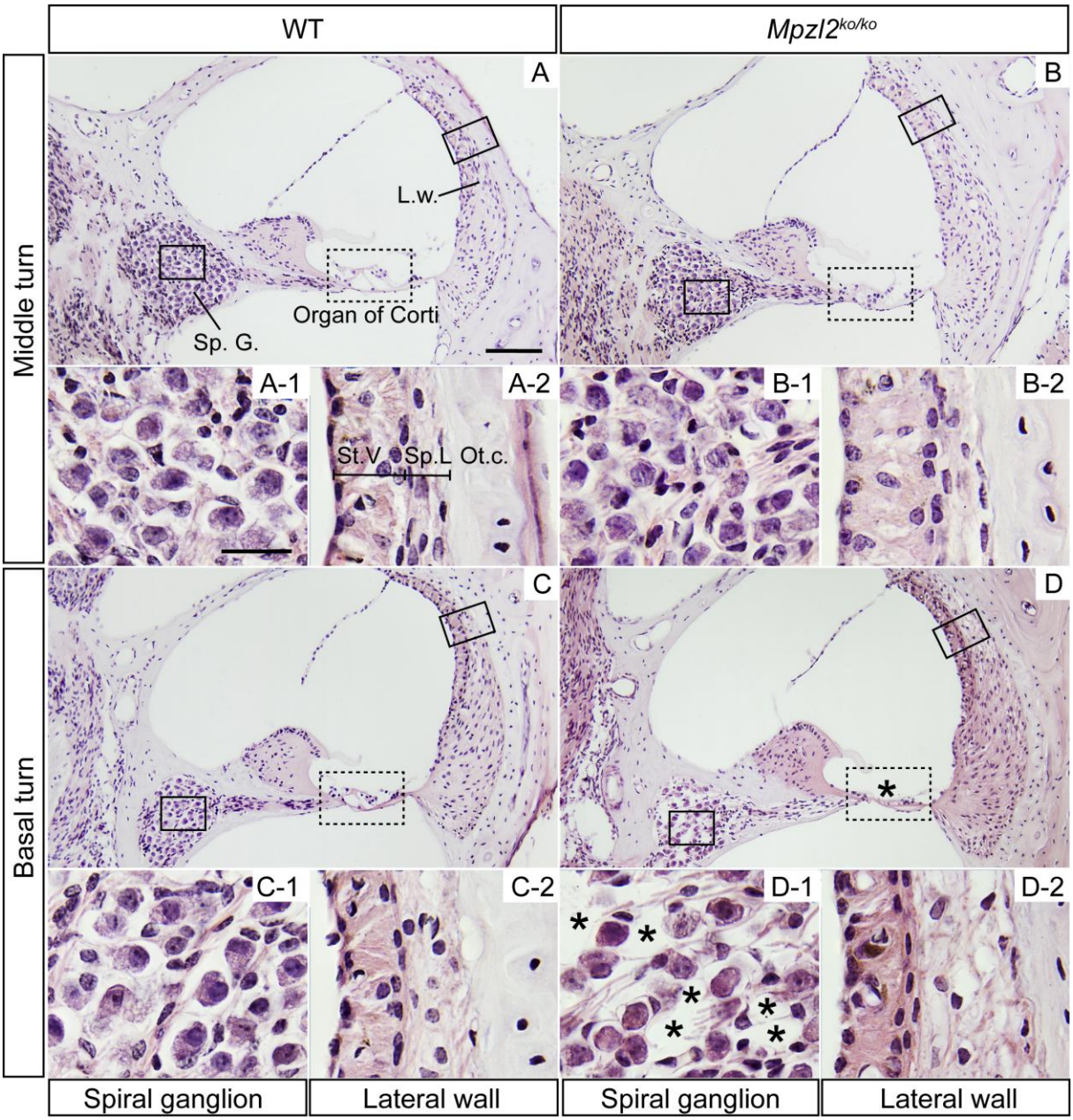

Figure S9. **Cochlear morphology of 12-week-old wild-type mice and *Mpzl2* (*Mpzl2*$^{ko/ko}$) mice**

Representative microphotographs from the middle (**A** and **B**) and basal (**C** and **D**) cochlear turns from midmodiolar cross sections. The second and fourth rows include close-ups of the boxed areas, from left to right: spiral ganglion (1), and stria vascularis (2). Asterisks mark abnormalities. L.w., lateral wall; Ot.c., otic capsule; Sp.G., spiral ganglion; Sp.L., spiral ligament; St.V., stria vascularis. Scale bar A-D, 100 µm, close-ups 25 µm.

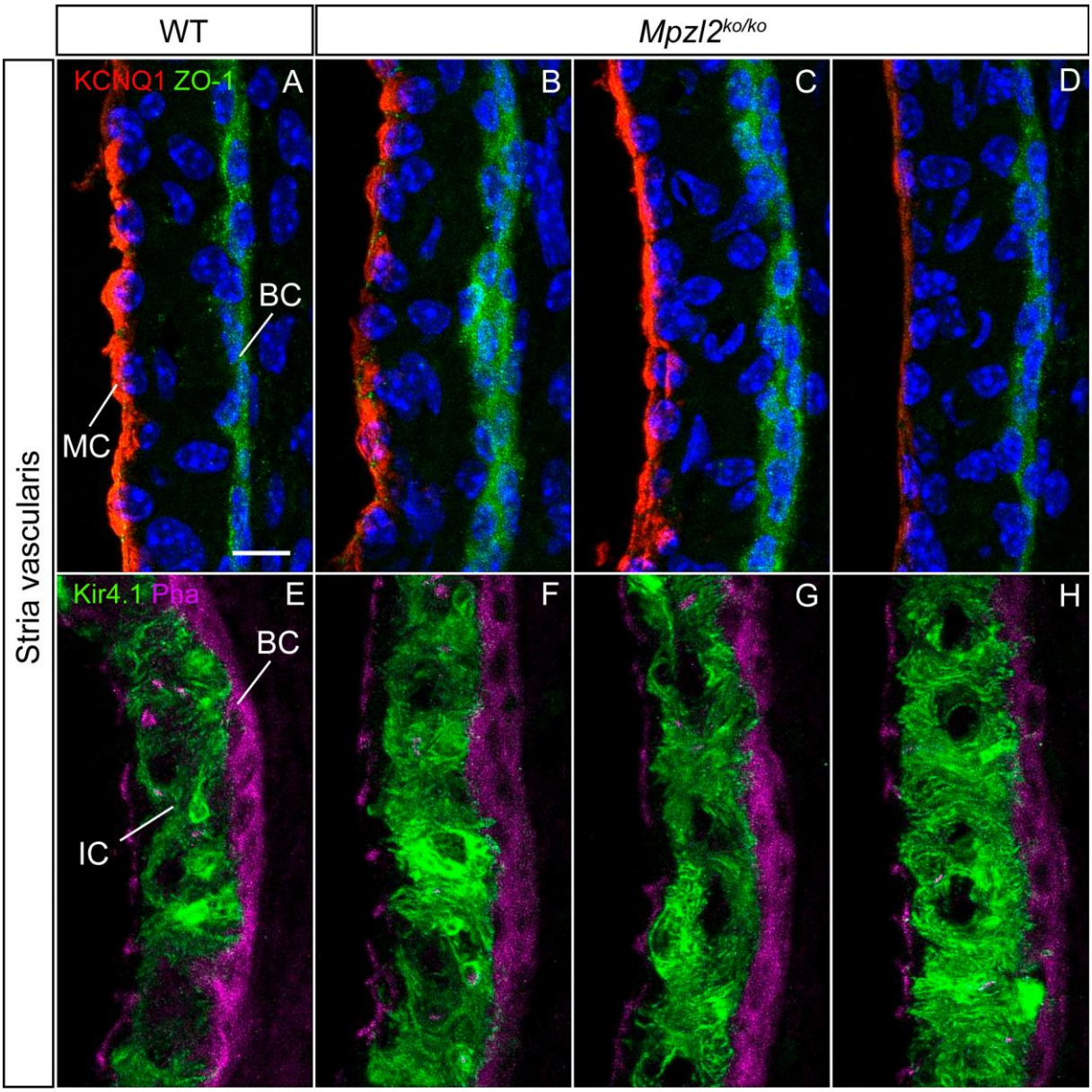

Figure S10. Normal cellular organization of the stria vascularis in wild-type mice and *Mpzl2* (*Mpzl2*$^{ko/ko}$) mice

Close-ups of the stria vascularis (**A-H**) of the basal turn of the cochlea from representative cryosections (10 µm) prepared from a wild-type mouse (**A, E**) and three *Mpzl2* mutant mice (**B-D, F-H**). Strial marginal (MC), basal (BC) and intermediate cells (IC) were immunostained for KCNQ1 (red), ZO-1 (green) (**A-D**) and Kir4.1 (green) (**E-H**) respectively. Actin in the stria vascularis was stained with phalloidin (purple). Scale bar A-H: 10 µm.

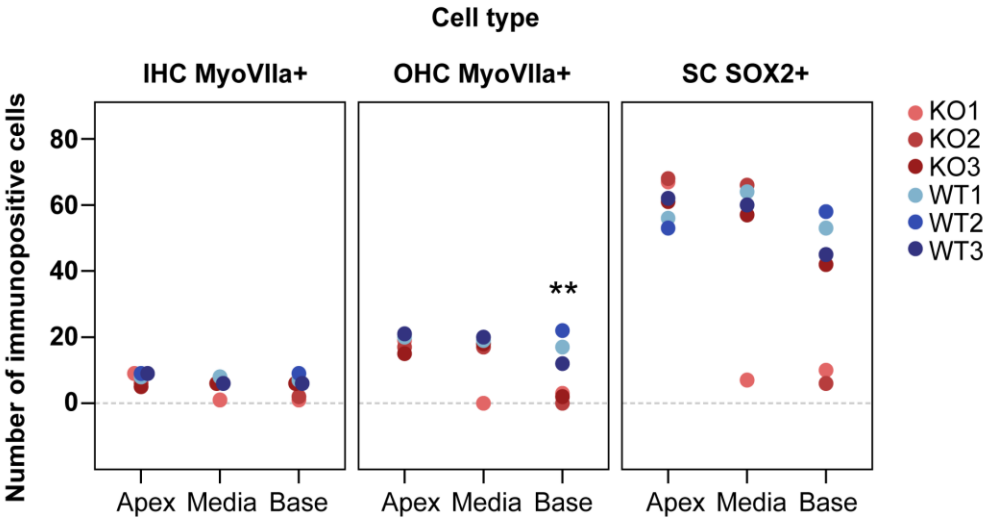

Figure S11. Quantification of MyoVIIa and SOX2 positive cells

Cell numbers were evaluated for wild-type (blue) and Mpzl2 (*Mpzl2*$^{ko/ko}$) mutant mice (red) for each turn of the cochlea. Data were obtained counting MyoVIIa and SOX2 positive cells in each cochlear region from 5 serial cryosections (10 µm) per animal (apex, n=3 mice per genotype in IHC and SC, n=2 wild-type, n= 3 KO in OHC; middle region, n= 2 wild-type, n=3 KO for each cell type; base, n=3 mice per genotype for each cell type). Data are expressed as the sum of each cell type per animal. Cochleae were derived from mice at 12 weeks of age. Statistical analysis was performed by Student t-test between groups for each marker and level of the cochlea. **p<0.01 (KO *versus* WT). IHC, inner hair cells; KO, *Mpzl2* mutant OHC, outer hair cells; SC, supporting cells.

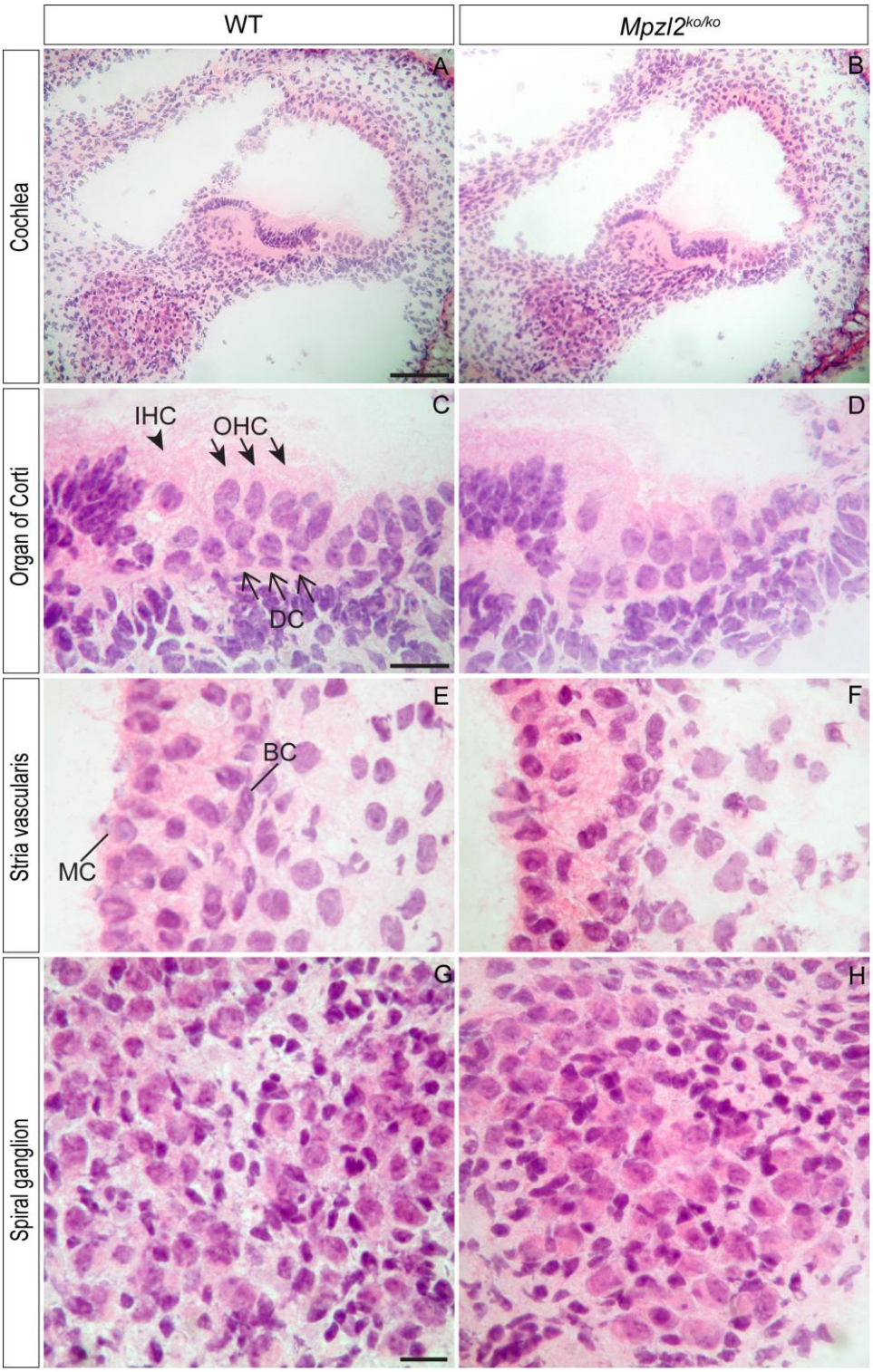

Figure S12. Normal histology of the cochlear basal turn at P4 in wild-type and mutant (*Mpzl2*$^{ko/ko}$) mice

Overview of the basal turn of cochleae (**A, B**) and higher magnifications of organs of Corti (**C, D**), striae vascularis (**E, F**) and spiral ganglions (**G, H**). Arrowheads point to inner hair cells (IHC), blackhead arrows to outer hair cells (OHC) and arrows to Deiters cells (DC). BC, basal cells; MC, marginal cells; WT, wild-type. Scale bars A-B: 100 µm, C-F: 20 µm and G, H: 20 µm.

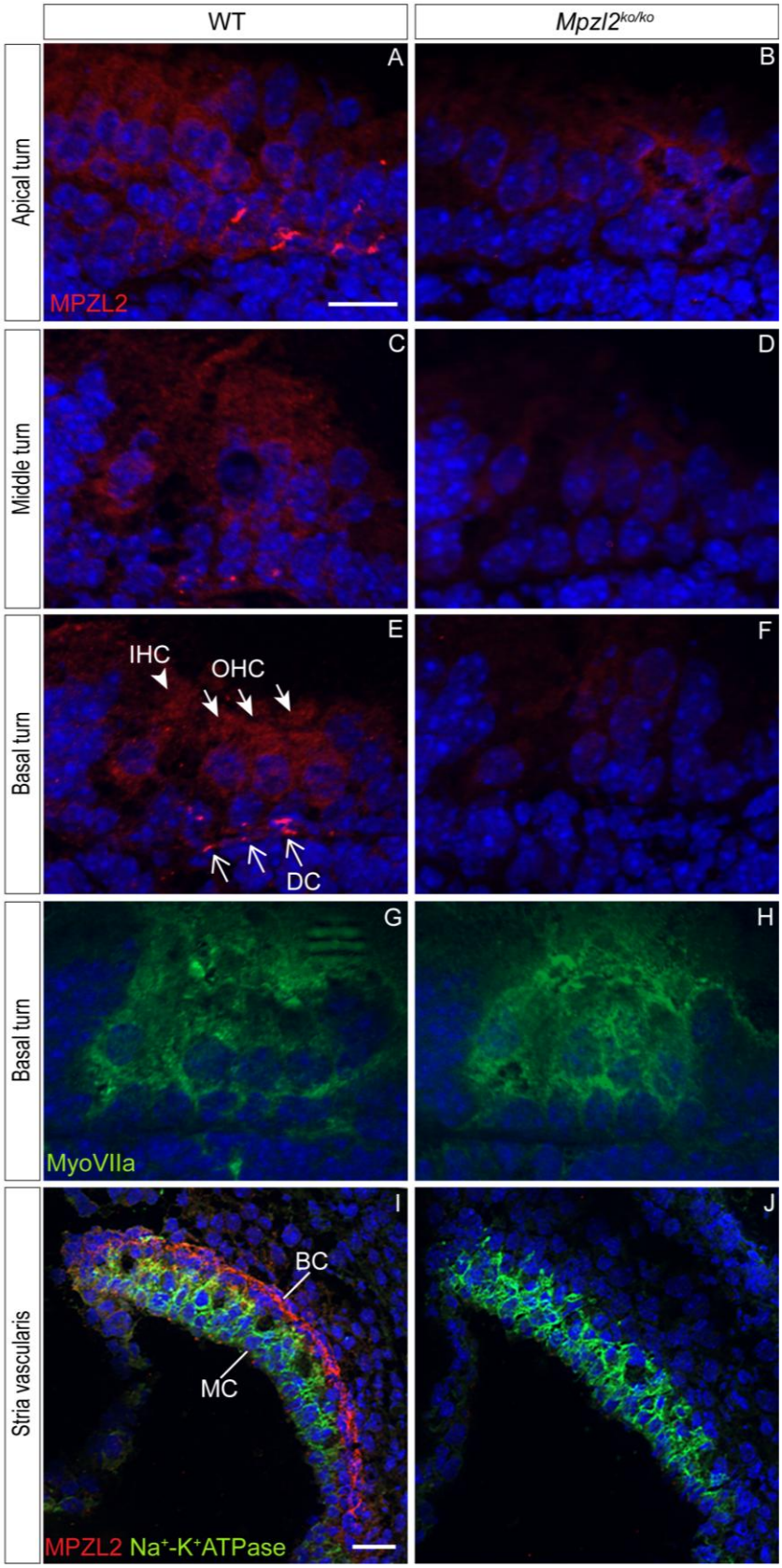

Figure S13. Specificity of immunostaining of MPZL2 in hair cells and Deiters cells of the organ of Corti and basal cells of the stria vascularis in P4 wild-type and Mpzl2 mutant (*Mpzl2*$^{ko/ko}$) mice Immunostaining of MPZL2 (red) is observed diffusely in the hair cells and Deiters cells and with higher intensity at the basal part of the Deiters cells in the

apical (**A**), middle (**C**) and basal (**E**) turns of the cochlea in wild-type mice. Antibody-specificity is confirmed by absence of immunostaining in these cells in the apical (**B**), middle (**D**) and basal (**F**) turns in *Mpzl2* mutant mice. Myosin VIIa (green) immunostaining shows the inner and outer hair cells of the organ of Corti in wild-type (**G**) and *Mpz2* mutants(**H**) mice. In the basal cells of the stria vascularis immunostaining of MPZL2 (red) was observed in the wild-type (**I**) mice and not in *Mpzl2* mutant (**J**) mice. Na^+/K^+-ATPase (green) immunostaining was employed for marking marginal cells (**I, J**). Cell nuclei were stained with DAPI (blue). IHC: inner hair cell, OHC: outer hair cell, DC: Deiters cell, MC: marginal cells, BC: basal cells. Scale bars A-H: 20 µm and I, J: 20 µm.

Supplemental Tables

Table S1. Primer sequences and PCR conditions
For primer design to amplify *MPZL2*, reference sequence NM_005797.3 was used, and for *TECTA*, ENST00000392793.

Table S2. Homozygous regions larger than 1 Mb and WES variants in family W05-682

Start SNP	End SNP	Chr	Start position	End position	Size (Mb)	Known deafness gene(s) in region	WES variants	Rare variants (MAF ≤ 1%)	Coding and splice site variants	(likely) pathogenic variants
rs4936310	rs10458997	11	110,900,760	134,746,130	23.85	*TECTA*	976	22	3	*MPZL2* c.72del
rs9910295	rs7406119	17	76,612,445	81,006,629	4.39	*ACTG1*	480	17	2	-
rs2353200	rs7835152	8	46,924,211	49,623,096	2.70	-	15	3	0	-
rs28870	rs803137	5	129,527,135	132,132,647	2.61	*SLC22A4*	75	1	0	-
rs7125329	rs1648142	11	107,895,836	109,870,952	1.98	-	59	2	0	-
rs10520657	rs12443195	15	88,114,594	90,071,734	1.96	-	62	0	-	-
rs9992997	rs17027362	4	132,958,066	134,644,433	1.69	-	6	0	-	-
rs2236047	rs9472138	6	42,126,399	43,811,762	1.69	-	102	5	0	-
rs4766455	rs12308836	12	109,641,578	111,287,959	1.65	-	42	6	0	-
rs7688203	rs17088085	4	66,568,856	68,057,322	1.49	-	0	0	-	-
rs2451256	rs10755578	6	159,507,338	160,969,738	1.46	-	145	1	0	-
rs1533075	rs9900927	17	63,039,373	64,423,010	1.38	-	37	2	0	-
rs8135828	rs5753355	22	29,929,239	31,259,658	1.33	-	66	2	0	-
rs7152200	rs8022938	14	66,836,155	67,855,327	1.02	-	7	1	0	-
rs7574269	rs6735340	2	14,700,457	15,705,915	1.01	-	59	1	0	-

Homozygous regions of shared genotypes. Genomic positions were determined using the UCSC Genome Browser, GRCh37/hg19 (https://genome.ucsc.edu/). The intronic variant of SLC22A4 (MIM: 604190; DFNB60) is not predicted to affect splicing. Coding and splice site base pairs of known deafness genes were covered by the indicated number of reads: TECTA ≥15; ACTG1 ≥15; SLC22A4 ≥20.

Table S3. Rare homozygous WES variants in family W05-682

Chr	Position	Ref	Var	AF_in house	Gnom AD_E AF NFE	Gene	Transcript	cDNA	Protein	CADD_ PHRED	SIFT	PPH2	Mutation Taster
chr6	90383869	C	T	0.28	0.43	*MDN1*	NM_014611.2	c.13201G>A	p.Val4401Ile	2.38	0.00	0.002	Disease causing
chr6	99729213	T	C	0.18	0.13	*FAXC*	NM_032511.3	c.1057A>G	p.Lys353Glu	13.22	0.05	0.040	Disease causing
chr6	116943955	G	A	0.02	0.00	*RSPH4A*	NM_001010892.2	c.711G>A	p.=	8.44	-	-	-
chr8	8176387	C	G	0.32	-	*SGK223*	NM_001080826.2	c.3498G>C	p.=	0.02	-	-	-
chr11	640090	G	C	0.98	-	*DRD4*	NM_000797.3	c.841G>C	p.Ala281Pro	9.47	1.00	0.000	Polymorphism
chr11	**118133799**	**T**		**0.13**	**0.14**	***MPZL2***	**NM_005797.3**	**c.72del**	**p.Ile24Metfs***	16.91	-	-	-
chr11	**122850170**	**A**	**G**	**0.06**	**0.00**	***BSX***	**NM_001098169.1**	**c.263-5T>C**	**p.?**	8.18	-	-	-
chr11	**123479372**	**G**	**A**	**0.26**	**0.24**	***GRAMD1B***	**NM_001286563.1**	**c.1111G>A**	**p.Val371Ile**	17.82	0.09	0.206	Disease causing
chr17	39340843	G	A	0.17	0.29	*KRTAP4-1*	NM_033060.2	c.264C>T	p.=	4.66	-	-	-
chr17	39340852	G	A	0.10	0.30	*KRTAP4-1*	NM_033060.2	c.255C>T	p.=	8.95	-	-	-
chr17	79082774	C	T	0.16	0.25	*BAIAP2*	NM_017450.2	c.1542C>T	p.=	9.92	-	-	-
chr17	80395141	T	C	0.04	0.00	*HEXDC*	NM_173620.2	c.801T>C	p.=	0.45	-	-	-
chr19	53117017	T	G	-	-	*ZNF83*	NM_001105549.1	c.801A>C	p.=	0.04	-	-	-

Variants indicated in bold are in the shared 23.85 Mb homozygous region of chromosome 11 and co-segregated with the HI in the family. Variants of *MDN1* and *FAXC* did not segregate with the disease. For none of the variants an effect on transcript splicing was predicted and none of the variants was present in the ClinVar database. Genomic positions are according to GRCh37/hg19. AF_inhouse (%) represent allele frequencies in the in-house database of ~15,000 exomes. Gnom AD_E AF NFE, allele frequency (%) in GnomAD, exomes of non-Finnish Europeans; PPH2, PolyPhen-2. Scores that meet the thresholds for pathogenicity as indicated in ‘Subjects and Methods’ are indicated in red.

Table S4. WES variants of *TECTA* in family W05-682

Chr	Position	Ref	Var	AF_in house	Gnom AD_E AF NFE	Gnom AD_G AF NFE	cDNA	Protein	PhyloP	CADD_ PHRED	SIFT	MutationTaster	PPH2	ClinVar
chr11	120976413	G	A	39.67	-	39.47	c.65-127G>A	p.?	0.872	8.62	-	-	-	-
chr11	120976428	A	G	49.35	-	48.75	c.65-112A>G	p.?	-2.755	0.89	-	-	-	-
chr11	120984087	C	G	23.51	-	26.46	c.624+169C>G	p.?	-1.978	0.41	-	-	-	-
chr11	120989335	A	G	39.81	41.30	42.88	c.1111A>G	p.Arg371Gly	4.856	3.89	1.00	Polymorphism	0.000	UV1
chr11	121007948	C	T	18.69	-	-1.00	c.2942-182C>T	p.?	-1.365	0.21	-	-	-	-
chr11	121016098	T	C	19.33	-	20.93	c.3544-166T>C	p.?	0.401	15.71	-	-	-	-
chr11	121016145	G	A	20.10	-	20.92	c.3544-119G>A	p.?	-0.469	7.34	-	-	-	-
chr11	121016818	G	A	20.14	21.15	20.95	c.4098G>A	p.=	-3.629	3.59	-	-	-	UV1
chr11	121016838	C	T	19.32	20.75	20.48	c.4105+13C>T	p.?	0.784	3.22	-	-	-	UV1
chr11	121023992	A	G	14.95	-	33.67	c.4305+203A>G	p.?	-0.213	8.36	-	-	-	-
chr11	121033105	A	G	35.76	34.46	33.76	c.5272+26A>G	p.?	0.172	8.76	-	-	-	-
chr11	121033277	C	T	18.95	-	33.65	c.5272+198C>T	p.?	-0.867	6.61	-	-	-	-
chr11	121035860	G	T	33.99	-	33.63	c.5273-122G>T	p.?	-0.110	6.56	-	-	-	-
chr11	121037530	G	A	20.14	20.91	20.70	c.5586+41G>A	p.?	1.650	11.75	-	-	-	-
chr11	121037554	T	C	20.03	-	20.67	c.5586+65T>C	p.?	0.044	7.73	-	-	-	-
chr11	121039234	T	C	18.35	-	20.63	c.5751-152T>C	p.?	0.251	8.22	-	-	-	-

For none of the variants an effect on transcript splicing is predicted. Genomic positions are according to GRCh37/hg19. AF_inhouse (%) represent allele frequencies in the in-house database of ~15,000 exomes; Gnom AD_E AF NFE, allele frequency (%) in Gnom AD, exomes of non-Finnish Europeans; Gnom AD_G AF NFE, allele frequency (%) in Gnom AD, genomes of non-Finnish Europeans; PPH2, PolyPhen-2. PhyloP represents the phyloP100way score. Effect on cDNA is based on transcript NM_005422.2.

Table S5. Analysis of intragenic deletions in subjects with a heterozygous variant in *MPZL2*

Sample	Identified heterozygous variant	Gender	Mean Ct value *MPZL2* exon 2	Mean Ct value *MPZL2* exon 3	Mean Ct value *MPZL2* exon 5	Mean Ct value *SLC16A2* exon 6
DNA11-22171	c.544C>T (p.(Arg182*)), exon 4	female	25	24	25	24
DNA11-23140	c.268C>T (p.(Arg90Trp)), exon 3	male	25	24	25	25
Control		female	25	24	25	24

In two individuals of the phenotype-based cohort, rare mono-allelic variants of *MPZL2* were identified. As no variants could be detected of the second allele by Sanger sequencing, genomic qPCR was performed to identify possible intragenic deletions. qPCR was performed for exons without a heterozygous SNP (*MPZL2* exons 2, 3 and 5). Temperatures and reaction times for qPCR were as follows: 10 min at 95 °C, followed by 40 cycles of 15 sec at 95 °C and 30 sec at 60 °C. qPCRs were performed with the Applied Biosystem Fast 7900 System in accordance with the manufacturer's protocol (Applied Biosystems, Foster City, CA, USA). *SLC16A2* (MIM: 300095) was employed as a reference gene. All reactions were performed in duplicate, mean Ct values are indicated. These Ct values do not provide any indication for the presence of intragenic deletions encompassing exons 2, 3, or 5 of *MPZL2.*

Table S6. Shared rare homozygous and compound heterozygous WES variants in family W16-0451

Chr	Position	Ref	Var	AF_in house	Gnom AD_E AF	Gnom AD_G AF	Gene	Transcript	cDNA variant	Protein variant	CADD_ PHRED	SIFT	PPH2	MutationTaster
								Homozygous						
chr1	14105151	TGA		0.60	-	0.34	*PRDM2*	NM_012231.4	c.861_863del	p.Asp287del	12.41	-	-	-
chr16	69988459	T	G	0.19	0.03	0.01	*CLEC18A*	NM_182619.3	c.439T>G	p.Cys147Gly	15.91	0.02	0.357	Disease causing
								Compound heterozygous						
chr1	228404296	C	T	0.00	-	0.01	*OBSCN*	NM_001271223.2	c.2270C>T	p.Ser757Leu	4.84	0.01	0.005	Polymorphism
chr1	228526578	T	A	0.83	0.81	0.84	*OBSCN*	NM_001271223.2	c.19980T>A	p.Ser6660Arg	18.55	0.00	0.690	Polymorphism
chr6	168315860	A	G	0.00	-	0.00	*AFDN*	NM_001291964.1	c.2168A>G	p.His723Arg	14.37	0.00	0.273	Disease causing
chr6	168317830	C	G	0.00	0.00	0.00	*AFDN*	NM_001291964.1	c.2483C>G	p.Thr828Ser	26.10	0.02	0.803	Disease causing
chr11	118133799	T	-	0.13	0.08	0.04	*MPZL2*	NM_005797.3	c.72del	p.Ile24Metfs*	16.91	-	-	-
chr11	118133651	G	A	0.02	0.04	0.04	*MPZL2*	NM_005797.3	c.220C>T	p.Gln74*	39	-	-	-
chr14	104433097	A	G	0.20	0.27	0.43	*TDRD9*	NM_153046.2	c.694A>G	p.Thr232Ala	16.61	0.00	0.558	Disease causing
chr14	104497541	C	T	0.00	0.00	-	*TDRD9*	NM_153046.2	c.3379C>T	p.Leu1127Phe	9.49	0.07	0.698	Polymorphism
chr22	26173565	C	T	0.00	0.01	0.03	*MYO18B*	NM_001318245.1	c.1885C>T	p.Arg629Trp	13.02	0.01	0.007	Polymorphism
chr22	26422656	C	G	0.02	0.02	0.02	*MYO18B*	NM_001318245.1	c.6719C>G	p.Ser2240Trp	18.35	0.00	0.878	Polymorphism

Genomic positions are according to GRCh37/hg19. For none of the variants an effect on transcript splicing is predicted and none of the variants is present in ClinVar**.** AF_inhouse is indicated in %. Gnom AD_E AF, allele frequency (%) in Gnom AD, exomes; Gnom AD_G AF, allele frequency (%) in Gnom AD, genomes; PPH2, PolyPhen-2. Scores that meet the thresholds for pathogenicity are indicated in red. Only the homozygous variant of *PRDM2* co-segregated with the disease.

Table S7. Individual results of otoscopy, tympanometry, pure-tone audiometry, OAEs, acoustic reflexes, HI progression and speech discrimination

Family	Subject	Age at evaluation (years)	Reported onset age of HI (years)	Otoscopic examination	Tympano-metry	PTA (dB HL)	OAEs	Mean ART	Statistically significant progression of HI (follow-up)	SRT (dB)	Maximum SRS (%)
W05-682	II:1	37	4	normal	R+L type A	60	R+L ND	100 dB	yes (21 years)	50	100
	II:3	42	9	R+L myringo-sclerosis	R+L type A	65	R+L ND	100 dB	yes (20 years)	53	100
	III:2	9	4	normal	R+L type A	37	R+L ND	90 dB	no (4 years)	32	90
W16-0195	II:1	8	3	normal	R type A L type Ad	40	R+L ND	90 dB	no (3 years)	30	100
W16-0451	I:2	44	childhood	normal	R+L type A	48	R+L ND	90 dB	yes (10 years)	31	92
	II:1	13	3	NT	NT	35	NT	NT	no (7 years)	NT	NT
	II:2	16	5	normal	R+L type A	38	R ND L detected at 1 kHz	90 dB	no (5 years)	27	95
	II:3	7	6	normal	R+L type A	35	R+L detected at 1.4kHz	90 dB	no (1 year)	28	95

PTA, pure tone average, mean thresholds of 0.5, 1 and 2 kHz in dB HL; OAEs, otoacoustic emissions; ART, acoustic reflex threshold; SRT, speech reception threshold; SRS, speech recognition score; R, right; L, left; ND, not detected; NT, not tested. Tympanometry type A means a normal curve, indicating normal pressure in the middle ear with normal mobility of the eardrum and ossicles; type Ad means a higher curve, indicating increased mobility of the eardrum and/or ossicles. Progression of HI was considered significant if at least 2 frequencies showed significant progression ($p \leq 0.05$). Results of audiometry, acoustic reflexes and speech discrimination from the better hearing ear are presented. One of the siblings (II:1) of family W16-0451 was not able to participate in the clinical evaluation; only retrospective data of this subject were used for analysis.

Table S8. Individual results of ABR and vestibular tests

Family	Subject	Click-evoked ABR	History of vestibular symptoms	Rotary chair test	Caloric irrigation test	vHIT	cVEMP
W05-682	II:1	symmetric, normal wave latencies	no	normal	normal	normal	normal (slightly lower)
	II:3	NT	no	NT	NT	NT	NT
	III:2	NT	no	NT	NT	NT	NT
W16-0195	II:1	symmetric, normal wave latencies	no	NT	NT	NT	NT
W16-0451	I:2	NT	two periods of vertigo in the past, without persisting complaints	normal	normal	normal	normal (slightly lower)
	II:1	NT	unknown	NT	NT	NT	NT
	II:2	NT	no	normal	slight asymmetry to the detriment of the left vestibulum	normal	normal (slightly lower)
	II:3	NT	no	NT	NT	NT	NT

ABR, auditory brainstem response; vHIT, video head impulse test; cVEMP, cervical vestibular evoked myogenic potentials; NT, not tested.

Supplemental Methods

Screening protocol for polyneuropathy in subjects with *MPZL2* variants

Medical history was obtained regarding sensory disturbances, muscle weakness, functional impairment (walking, walking stairs, cycling), and use of medication. Participants also underwent physical neurological examination.

Neurological examination included testing of:

- Cranial nerves, according to current standards
- Muscle strength using the Medical Research Council (MRC) scores (0-5) of 18 predefined muscle groups, including shoulder abduction, elbow flexion, wrist extension, hip flexion, knee extension, foot dorsiflexion (extension) and plantar flexion, and toe dorsiflexon (extension); muscle tone and bulk
- Muscle mass of the extensor digitorum brevis muscle (normal / atrophic)
- Vigorimeter grip strength, as described previously[3]
- Coordination with use of nose-finger test and tandem gait (normal / abnormal).
- Sensation, using the Modified INCAT Sensory Sum Score (mISSReflexes) and the Romberg test (1= abnormal; 0 = normal), according to the European Federation of Neurological Societies/Peripheral Nerve Society guideline on management of chronic inflammatory demyelinating polyradiculoneuropathy[4]
- Deep tendon reflexes (biceps, triceps, patellar and ankle jerks) bilaterally (absent / reduced / normal)

Screening for immunological defects and defects of the cornea and vision

Immunological screening was performed to evaluate presence of immunodeficiencies by asking participants about symptoms of allergies, autoimmune diseases, and frequent, prolonged or severe infections or inflammations. In addition, the numbers of CD4- and CD8-expressing human T cells were analyzed, using flow cytometry, as indicated in the legend of Figure S7. Screening for corneal abnormalities and vision problems was performed by history, slit lamp biomicroscopy and evaluation of visual acuity using a Snellen chart.

In silico evaluation of missense variants and prediction of effects on splicing

Prediction of a potential pathogenic effect of missense variants was performed with CADD PHRED[5] (≥15), SIFT (≤0.05), PolyPhen-2 (PPH2, ≥0.450) and Mutation Taster[6] (deleterious). Values for predicted pathogenicity are indicated between brackets. Segregation analysis was performed if at least two of the tools predicted a pathogenic effect of the variant. In case of more than one rare heterozygous variant in a gene, segregation analysis was performed if the pathogenicity criteria were met for one of the variants. A potential effect on splicing was predicted with the tools SpliceSiteFinder-like, MaxEntScan, NNSPLICE, GeneSplicer, and Human Splicing Finder as available in Alamut Visual (version 2.10, Interactive Biosoftware, Rouen, France). A change of at least 30% of splice site scores in at least two of the tools was regarded significant. Also PPH2 and SIFT were employed via Alamut Visual.

Quantitative PCR (qPCR) analysis for identification of intragenic deletions

We quantified copy numbers of *MPZL2* exons 2, 3 and 5 by using genomic qPCR. Specific primers (Table S1) were designed with Primer3Plus and reference sequence NM_005797.3. qPCRs were performed with 5 *μ*g genomic DNA and reaction mixtures were prepared with the GoTaq qPCR Master Mix (Promega) in accordance with the manufacturer's protocol. qPCRs were performed with the Applied Biosystem Fast 7900 System in accordance with the manufacturer's protocol (Applied Biosystems). *SLC16A2* (MIM: 300095) was employed as a reference gene. All reactions were performed in duplicate.

Histology and immunohistochemistry of cochleae from wild-type and *Mpzl2* mutant mice

Cochleae from 12 weeks old mice (n=3 per genotype) were dissected, decalcified and embedded in paraffin or Tissue-Tek OCT (Sakura Finetek). Deparaffinized cochlear sections (5 μm) were stained with hematoxylin and eosin, and images for general cytoarchitecture evaluation were taken with 10x, 20x and 40x magnification objectives with an Olympus DP70 digital camera as described previously.[7] For immunofluorescence assays of 12-week cochleae, cryosections (10 μm) were treated overnight at 4ºC with the following primary antibodies: rabbit anti-Kir4.1 (1:200 AB5818 Chemicon), rat anti-ZO-1 (1:200 sc-33725 Santa Cruz); rabbit anti-KCNQ1 (1:200 sc-20816 Santa Cruz), rabbit anti-Myosin VIIa (1:250 25-6790 Proteus), or goat anti-SOX2 (1:100 sc-17320 SantaCruz). After washing, sections were incubated with the corresponding secondary Alexa conjugated antibodies for 2 hrs at room temperature (RT), essentially as reported in Sanchez-Calderon *et al.* (2010).[8]

Images were taken with epifluorescence (Nikon 90i, Tokyo, Japan) and/or confocal (Leica TCS SP2; Leica, Wetzlar, Germany) microscopes. SOX2 and Myosin VIIa positive cells were counted from base to apex in five serial cryosections (10 μm) per animal separated by 50 μm, prepared from 3 mice of each genotype. The intensities of KCNQ1, ZO-1, and Kir4.1 immunostainings were determined in areas of the stria vascularis, delimited by thresholding the marker's fluorescent signal using Fiji software v1.51n (National Institutes of Health, Bethesda, MD, USA). The fluorescence optical density was thus determined from base to apex in 3-5 serial cryosections (10 μm) per animal separated by 50 μm, prepared from 3 mice of each genotype. Statistical significance was determined by Student's t test for unpaired samples.

For evaluation of early postnatal cytoarchitecture of the cochlea and for localization of MPZL2, inner ears of postnatal day four (P4) C57BL6J wild-type and *Mpzl2* mutant mice (n=3) were dissected, cryoprotected with 10% sucrose in PBS before embedding in Tissue-Tek OCT. For analysis of the cytoarchitecture, cryosections (7 μm) were fixed with paraformaldehyde (PFA) 4% (10 min), stained with hematoxylin and eosin, and analyzed on a Zeiss Axioskop light microscope. For immunofluorescence, cryosections were permeabilised with 0.01% Tween20 in PBS (20 min) and after rinsing with PBS and blocking with blocking buffer (ovalbumin 0.1% and fish gelatin 0.5% in PBS; 1 hr) incubated overnight at 4 ºC with primary antibodies diluted in blocking buffer. After rinsing with PBS, cryosections were incubated (1 hr) with secondary antibodies diluted in blocking buffer with DAPI (1:8000; D1306; Molecular Probes). After rinsing in PBS, sections were fixed in PFA 4% in PBS (10 min), rinsed and mounted in anti-fade Prolong Gold (P36930; Molecular Probes). Analyses were performed on a Zeiss Axio Imager fluorescence microscope and for higher resolution on a Zeiss LSM880 confocal microscope. As primary antibodies were used: Rabbit anti-MPZL2, raised against the complete protein (1:200 11787-1-AP Proteintech,), rabbit anti-

Myosin VIIa (1:200 25-6790 Proteus), goat anti-Collagen IV (1:200 1340-01 SouthernBiotech), and mouse anti-Na^+-K^+ATPase α1 (1:5 α6F Developmental Studies Hybridoma Bank). As secondary antibodies were utilized: Alexa Fluor (AF) conjugated immunoglobulins (Molecular Probes): AF 568-goat anti-rabbit (A11011), AF 488-donkey anti-goat (A11055), AF 488-goat anti-mouse (A11029) and AF 488-goat anti-rat (A11006), at a 1:800 dilution.

Supplemental References

1. Seelow D, Schuelke M, Hildebrandt F, Nurnberg P. HomozygosityMapper--an interactive approach to homozygosity mapping. *Nucleic Acids Research.* 2009;37(Web Server issue):W593-599.
2. Pfaffl MW. A new mathematical model for relative quantification in real-time RT-PCR. *Nucleic Acids Research.* 2001;29(9):e45.
3. Vanhoutte EK, Latov N, Deng C, et al. Vigorimeter grip strength in CIDP: a responsive tool that rapidly measures the effect of IVIG--the ICE study. *European Journal of Neurology.* 2013;20(5):748-755.
4. Van den Bergh PY, Hadden RD, Bouche P, et al. European Federation of Neurological Societies/Peripheral Nerve Society guideline on management of chronic inflammatory demyelinating polyradiculoneuropathy: report of a joint task force of the European Federation of Neurological Societies and the Peripheral Nerve Society - first revision. *European Journal of Neurology.* 2010;17(3):356-363.
5. Kircher M, Witten DM, Jain P, O'Roak BJ, Cooper GM, Shendure J. A general framework for estimating the relative pathogenicity of human genetic variants. *Nature Genetics.* 2014;46(3):310-+.
6. Schwarz JM, Cooper DN, Schuelke M, Seelow D. MutationTaster2: mutation prediction for the deep-sequencing age. *Nature Methods.* 2014;11(4):361-362.
7. Martinez-Vega R, Garrido F, Partearroyo T, et al. Folic acid deficiency induces premature hearing loss through mechanisms involving cochlear oxidative stress and impairment of homocysteine metabolism. *FASEB Journal.* 2015;29(2):418-432.
8. Sanchez-Calderon H, Rodriguez-de la Rosa L, Milo M, Pichel JG, Holley M, Varela-Nieto I. RNA microarray analysis in prenatal mouse cochlea reveals novel IGF-I target genes: implication of MEF2 and FOXM1 transcription factors. *PLoS One.* 2010;5(1):e8699.